A new criterion for determining the representative elementary volume of translucent porous media and inner contaminant

Ming Wu[1, 2], Jianfeng Wu[2*], Jichun Wu[2], and Bill X. Hu[1*]

[1] Institute of Groundwater and Earth Sciences, Jinan University, Guangzhou 510632, China

[2] Key Laboratory of Surficial Geochemistry, Ministry of Education; Department of Hydrosciences, School of Earth Sciences and Engineering, Nanjing University, Nanjing 210023, China

Correspondence to: J.F. Wu (jfwu@nju.edu.cn), B.X. Hu (billhu@jnu.edu.cn)

ABSTRACT

Representative elementary volume (REV) is essential to measure and quantify the effective parameters of a complex heterogeneous medium. To overcome the limitations of the existing REV estimation criteria~~Since previous REV estimation criteria having multiple limitations~~, a new REV estimation criterion (χ^i) based on dimensionless range and gradient calculation is proposed in this study to estimate REV of a translucent material based on light transmission techniques. ~~Two~~ Three sandbox experiments are performed to estimate REVs of porosity, density, tortuosity and perchloroethylene (PCE) plume using multiple REV estimation criteria. In comparison with χ^i, previous REV estimation criteria based on the coefficient of variation (~~C_V^i~~ C_V^i), the entropy dimension (DI^i ~~DI^i~~) and the relative gradient error (ε_g^i ~~ε_g^i~~) are tested in REV quantification of translucent silica and inner PCE plume to achieve their corresponding effects. Results suggest that new criterion (χ^i) can effectively identify the REV in the materials, whereas the coefficient of variation ~~(C_V^i)~~ and entropy dimension (DI^i) ~~cannot~~are not effective. The relative gradient error ~~(ε_g^i)~~ can make the REV plateau obvious, while random fluctuations make the REV plateau uneasy to identify accurately. Therefore, the new criterion is appropriate for REV estimation for the translucent materials and inner contaminant. Models are built based on Gaussian equation to simulate the distribution of REVs for media properties, which frequency of REV is dense in the middle and sparse on both sides. REV estimation of PCE plume indicates high level of porosity lead to large value of mean and standard deviation for REVs of PCE saturation (S_o) and PCE-water interfacial area (A_{OW}). Fitted equations are derived for distribution of REVs for PCE plume related to d_m (distances from mass center to considered point) and d_I

(distances from injection position to considered point). Moreover, relationships between REVs of PCE plume and S_o are fitted using regression analysis. Results suggest a decreasing trend appears for S_o-REV when S_o increases, while A_{ow}-REV increases with increasing of S_o.

Keywords: new criterion; representative elementary volume (REV); translucent material

1. Introduction

Modelling groundwater and contaminant (such as hazardous irons) transport in subsurface environment is based on the premise that micro-structure of aquifer exist a representative elementary volume (REV) (Wang et al., 2016; Lei and Shi, 2019). REV acts as a micro-scale characteristic, which is important to improve our understanding of materials, inner fluid flow and other processes (Brown and Hsieh, 2000; Costanza-Robinson et al., 2011; Wu et al., 2017). Previous studies suggested that even the Platinum-Nanoparticle-Catalyzed hydrogenation reactions and ion transport through angstrom-scale slits in cell activity existed apparent size effect, implying size effect is a wide characteristic for many process and materials (Bai et al., 2016; Esfandiar et al., 2017). With the help of REV, a porous medium can be treated as continuum medium (Brown and Hsieh, 2000; Kang et al., 2003; Müller and Siegesmund, 2010; Teruel and Rizwan-uddin, 2010; Hendrick et al., 2012; Wang et al., 2012; Ukrainczyk and Koenders, 2014; Kim and Mohanty, 2016; Gilevska et al., 2019). A conceptual representation of "REV curve" (Brown and Hsieh, 2000), characterizing porosity ($n\theta$) change with measured scale (L) increment, is presented in Fig. 1ea. Based on the characteristic of REV curve in Fig. 1ae, the REV curve can be divided into three regions. When measured scale (Fig. 1b) is in region I, the porosity

fluctuates drastically at small scales. As measured scale size ranging between L_{min} and L_{max}, a flat plateau with constant and steady value is encountered and the property is factored into its average value. Material property in spatial scales less than L_{min} is spatially varied portions with small scale, which can be easily influenced by individual pores in micro-structure such as region I (Fig. 1~~e~~a). Likewise, material property is allowed drift to new values in spatial scale above L_{max} due to additional morphological structures of large field heterogeneity (region III). As a matter of fact, REV scale of region II can be derived between the small and spatially varied property in region I and large field variability in region III. However, the lower and upper boundaries L_{min} and L_{max} of REV plateau is hard to be identified in reality (Brown and Hsieh, 2000; Costanza-Robinson et al., 2011).

As technology advanced and progressed, non-destructive and non-invasive techniques of x-ray and gamma ray micro-tomography were utilized for micro-structure characteristic measurement in materials –(Ghilardi, 1993; Brown and Hsieh, 2000; Niemet and Selker, 2001; Bob et al., 2008; Al-Raoush and Papadopoulos, 2010; Costanza-Robinson et al., 2011; Al-Raoush, 2012; Borges and Pires, 2012; Fernandes et al., 2012; Rozenbaum and Roscoat, 2014; Pereira Nunes et al., 2016; Piccoli et al., 2019). Generally, REV estimation for material properties, inner gas and fluid also was usually implemented by micro visualization and scanning of X-ray and gamma ray in laboratory (Brown and Hsieh, 2000; Razavi –et al., 2007; Nordahl and Ringrose, 2008; Al-Raoush and Papadopoulos, 2010; Costanza-Robinson et al., 2011; Rozenbaum and Roscoat, 2014; Borges et al., 2018), while different criteria were utilized to quantify REV (Brown and Hsieh, 2000; Martínez et al., 2007; Nordahl and Ringrose, 2008; Costanza-Robinson et al., 2011). Lower boundary scale L_{min}

78 of REV was identified by means of entropy dimension (DI^i ~~DI^i~~) for eight soil samples
79 (Martínez et al., 2007). Further, REV scale of permeability for ripple laminated sandstone
80 intercalated with mudstone was estimated using the coefficient of variation (C_V^i ~~C_V^i~~), which
81 the REV scale is identified by the variability among the ten samples to achieve average
82 REV scale (Nordahl and Ringrose, 2008). As a result, only one REV boundary was
83 identified and not every sample can be estimated effectively (Nordahl and Ringrose,
84 2008). More interestingly, REV ~~scales for~~of material property (porosity), moisture
85 saturation and air-water interfacial areas in porous media were estimated by a criterion
86 named the relative gradient error (ε_g^i)(Costanza-Robinson et al., 2011). REVs of
87 permeability of translucent material, PCE saturation and PCE-water interfacial area also can
88 be estimated using the relative gradient error (Wu et al., 2017). In summary, the REV
89 estimation was made by multiple kinds of criteria, while the REV identification effects
90 of these criteria were not clear. What's more, these previous criteria estimate REV scale
91 unsatisfactorily that beginning and ending of REV plateau can't be identified
92 simultaneously for translucent porous media based on light transmission technique.
93 Therefore, new criterion which can identify REV plateau accurately is needed.

94 In this study, a new criterion (χ^i) for REV estimation is proposed to identify the REV
95 scale of the translucent silica and inner contaminant. ~~Two~~ Three perchloroethylene (PCE)
96 transport experiments are conducted in two dimensional (2D) sandboxes to test the effect of
97 different REV estimation criteria. Translucent silica is selected for associated REV analysis
98 due to its extensive utilization in laboratory experiment of exploring groundwater flow and
99 contaminant migration behavior in micro-structure of a sandy aquifer (Niemet and Selker,

2001; Bob et al., 2008; Costanza-Robinson et al., 2011). Moreover, translucent silica is also an important material applied in numerous industries (Bouvry et al., 2016). In laboratory experiments, translucent silica is packed in 2D sandboxes where porosity, density, tortuosity, PCE saturation are derived by light transmission technique (Fig. 1c~~a~~). Porosity and PCE saturation are selected as the representative variables to explore corresponding REV estimation by different criteria, which is very essential and significant for REV identification. Previous criteria such as the coefficient of variation (C_V^i ~~C_V^i~~), entropy dimension (DI^i ~~DI^i~~), the relative gradient error (ε_g^i ~~ε_g^i~~) and the new criterion-χ^i are tested in REV estimation. Associated effects are analyzed to achieve the best criterion of effective and appropriate quantification of REV.

2. Experiment procedure and method

2.1 Experiment

~~Two~~ Three sandboxes (Fig. 2a~~-c and b~~) packed by translucent silica medium are prepared in laboratory to test different criteria of REV quantification. PCE is selected as a typical DNAPL contaminant used in experiments. 2D sandbox is composed by three aluminum interior frames and two glass walls, which thickness is 1.6cm. The dimensions of sandboxes used in Experiment~~s~~-I ~~and II~~ are 20 (width) ×15 (height), and the dimensions of Experiments-II and III ~~and~~ are 60 (width)×45 (height). F40/50 and F20/30 mesh translucent silica sands are used for background material for Experiments-I and II, while heterogeneous translucent silica with low porosity and permeability are packed in sandbox for Experiment-III. To make the translucent silica fully saturated by water in a flow field close to natural groundwater environment (Erning et al., 2012), water flow at flow velocity of 0.5 m/d is set

from left to right in laboratory sandbox experiments (Fig. 2a-c ~~and b~~). Water is restricted in a sandbox that the top and bottom layers of sandbox are packed by F70/80 mesh translucent silica as capillary barriers. Light source is placed behind the sandbox to make light penetrate through translucent media and capture emergent light intensity using a thermoelectrically air-cooled charge-coupled device (CCD) camera (Fig. 1c~~a~~). Afterward, PCE is injected into sandboxes from the injection needle at constant rate of 0.5 mL /min for ~~two~~ three experiments. Detailed experimental conditions are listed in Table 1.

2.2 Light transmission technique~~s~~

By means of light transmission technique (Fig. 1c~~a~~), DNAPL and water saturation can be obtained rapidly and in real-time, which greatly help to explore mechanism of groundwater flow and contaminant migration in porous media. When light passes through translucent materials of a given thickness, the emergent light intensity after the absorptive and interfacial losses can be expressed as (Niemet and Selker, 2001; Bob et al., 2008; Wu et al., 2017):

$$I_T = CI_0(\prod \tau_b)\exp(-\sum \alpha_a d_a) \quad (1)$$

where a represent phase number; b represent the number of the interface between phase a and a+1; I_0 is the original light intensity; C is a constant of correction for light emission and light observation; τ_{jb} is the transmittance when light penetrate from phase ja to aj+1; α_{ia} is the absorption coefficient when light penetrate in phase ia; d_{ia} is the length of light penetration path in phase ia.

To derive the porosity, the 2D translucent porous medium should be only saturated by water. Consequently, the emergent light intensity can be expressed as (Niemet and

Selker, 2001; Bob et al., 2008; Wu et al., 2017):

$$I_s = CI_0 \tau_{s,w}^{2k_o} \exp(-\alpha_s k_s d_s) \quad (2)$$

where $\tau_{s,w}^{2k_0}$ is the transmittance of solid-water interface; α_s is solid particles absorption coefficient; d_s is median diameter of the solid particles; k_o is the number of pores across light penetration path; k_s is the number of solid particles across light penetration path.

If we arbitrarily select an infinitesimal element, its area A_o approaches zero ($A_o \to 0$) from the 2D translucent porous media (Fig. 1d~~b~~), and suppose the infinitesimal element with thickness L_T containing solid particles and pores that can be regarded as lamellar structure (Fig. 1d~~c~~), we can obtain the following relationships (Wu et al., 2017):

$$\theta A_o L_T = A_o k_o d_o \quad (3)$$

$$k_s d_s + k_o d_o = L_T \quad (4)$$

where d_o is the median diameter of pores; θ is porosity.

Substituting Eq. (3) and Eq. (4) into Eq. (2), the relationship between emergent light intensity and porosity can be achieved (Wu et al., 2017):

$$\ln I_s = \beta + \theta\gamma \quad (5)$$

where $\beta = \ln(\frac{CI_s}{e^{\alpha_s d_s L_T}})$ and $\gamma = \ln(\tau_{s,w}^{\frac{2L_T}{d_0}} e^{\alpha_s L_T}) - \overline{\gamma = \ln(\tau_{s,w}^{\frac{2L_s}{d_o}} e^{\alpha_s L_T})}$. β and γ can be determined from experimental data, then porosity can be obtained.

The density and tortuosity are derived as (Wu et al., 2018):

$$\rho = \theta\rho_w + (1.0 - \theta)\rho_s \quad (6)$$

$$\tau = 1 + \frac{\pi - 2}{\sqrt{\frac{\pi}{1-\theta}}} \quad (7)$$

where ρ is the density of translucent porous media; ρ_w is the density of water; ρ_s is the

density of solid particles; τ is tortuosity .

The saturation of dense nonaqueous phase liquid (DNAPL) was quantified by light transmission technique based on light pass through translucent materials (Niemet and Selker, 2001; Bob et al., 2008):

$$S_o = \frac{\ln I_s - \ln I_T}{\ln I_s - \ln I_{oil}} \quad (8)$$

where S_o is the saturation of DNAPL; I_s is the light intensity after light penetration through translucent porous when all pores are fully saturated by water; I_{oil} is the light intensity when all pores are fully saturated by DNAPL; I_T is the light intensity after penetration through translucent materials. After quantification of PCE saturation, PCE-water interfacial area (A_{OW}) can be obtained based on the method proposed by Wu et al. (2017), where the unit of A_{OW} is cm^{-1}.

Emergent light intensity for three experiments are captured by a thermoelectrically air-cooled charge-coupled device (CCD) camera (Niemet and Selker, 2001; Bob et al., 2008). Every pixel with small scale could be approximated as infinitesimal element in high resolution image to apply light transmission techniques. As consequence, porosity of translucent silica was derived with light transmission technique through Eq. (5). The whole 2D translucent silica area was numerically discretized that every cell had the uniform dimensions of 0.015m×0.015m. The cuboid window (Fig. 1b) was utilized to quantify the variables (porosity, density, tortuosity, PCE saturation, PCE-water interfacial area) of every cell as measured scale was increased. In detail, the measured cuboid window scale was increased from the center of each cell and associated value of variable was calculated from the high resolution porosity of 2D translucent silica derived by light transmission technique.

Observation cells were selected from the discretized cells (Fig. 3b) of which the cells I-1~2, II-1~2 and III-1~2 belong to Experiments-I-III, respectively.

To analyze the regularity of REV distribution for PCE plume, the mass center coordinate and the granglia-to-pool ratio (GTP) of PCE plume for three experiments are quantified for Experiments-I-III. The mass center coordinate and GTP are calculated as:

$$X_m = \frac{M_{10}}{M_{00}} \quad (9)$$

$$Z_m = \frac{M_{01}}{M_{00}} \quad (10)$$

$$GTP = \frac{V_{ganglia}}{V_{pool}} \quad (11)$$

where X_m is x coordinate of mass center for PCE plume; Z_m is z coordinate of mass center for PCE plume; GTP is granglia-to-pool ratio, which equals to the ratio of the $V_{ganglia}$ to V_{pool}; $V_{ganglia}$ is the PCE volume under ganglia state; V_{pool} is the PCE volume under pool state; M_{00}, M_{10} and M_{01} are computed using definition of spatial moment (M_{ij}), $M_{ij} = \int_{x_0}^{x_1}\int_{z_0}^{z_1}\theta(x,z)S_o(x,z,t)x^i z^j d_x d_z$; x_0 and z_0 are minimum limits of x axis and z axis; x_1 and z_1 are maximum limits of x axis and z axis; θ(x,z) is the porosity at point (x,z); S_o(x,z,t) is PCE saturation of point (x, z) at time t.

2.3 Criteria of REV quantification

The REV is defined as the volume range in which all material characteristics are factored into the average and associated values approach single and constant (Brown and Hsiehs, 2000). In the range of REV, the value of one associated property will meet the condition:

$$\frac{\partial Y(L_i)}{\partial L}|_{L_i=L_o} = 0 \frac{\partial Y(L_i)}{\partial L}|_{L_i=L_o} = 0 \quad (12)$$

where the $Y(L_i)$ is the value of an associated property when system scale is L_i; L_i is the value of system scale; L_o is the scale range of REV, $L_{min}<L_o<L_{max}$; L_{max} is upper boundary of REV; L_{min} is lower boundary of REV scale. According to the Eq. (129), when the measured scale (L_i) reaches REV range, ~~the derivative~~ $\frac{\partial Y(L_i)}{\partial L} \rightarrow 0$ ~~$\frac{\partial Y(L_i)}{\partial L} \rightarrow 0$~~ ~~will tend to zero~~. As a matter of fact, most previously used criteria were applied to estimate REV based on this requirement~~. The REV estimation criteria tested in this study are illustrated in Table 2~~ (Brown and Hsieh, 2000; Martínez et al., 2007; Nordahl and Ringrose, 2008; Costanza-Robinson et al., 2011).

To evaluate the REV of porosity, the coefficient of variation (C_V^i ~~C_V^i~~) ~~(Table 2)~~ is utilized to estimate the variability (Nordahl and Ringrose, 2008):

$$C_V^i = \frac{\hat{s}_i}{\overline{\varphi}_i} \text{ ~~} C_V^i = \frac{\hat{s}_i}{\overline{\varphi}_i} \tag{130}$$

where i is the cuboid window (Fig. 1b~~b~~) increment number; ~~φ~~ φ is the measured variable, such as porosity; ~~$\hat{s}_i$~~ $\hat{s}_i$ is the standard deviation of sub-grids' variable in different measured volume or scale; ~~$\overline{\varphi}_i$~~ $\overline{\varphi}_i$ is the arithmetic average of the variable values in the sub-grids. When number of sub-grids (N) is less than 10, a correction is utilized to replace Eq. (130). According to Nordahl and Ringrose (2008), $0 < C_V^i < 0.5$ ~~$0 < C_V^i < 0.5$~~ is defined as homogeneous and $C_V^i = 0.5$ ~~$C_V^i = 0.5$~~ can be used as criterion to identify the REV scale.

Similarly, for porosity of translucent silica, entropy dimension (DI^i) ~~(Table 2)~~ is utilized for REV analysis and estimation (Martínez et al., 2007), which is defined as:

$$DI^i \approx \frac{\sum_{j=1}^{m(i)} \mu_j(L_\varepsilon) \log \mu_j(L_\varepsilon)}{\log L_\varepsilon} \tag{141}$$

where, L_ε is the scale of sub-grid; "≈" indicates the asymptotic equivalence as $L_\varepsilon \to 0$ (Martínez et al., 2007); j is the ordinal number of sub-grid in measured cuboid window (Fig. 1b) of increment number i; $m(i)$ is the total number of sub-grids in measured cuboid window (Fig. 1b) of increment number i; $\mu_j(\varepsilon)$ is the proportion of the variable of sub-grid j in the whole measured cuboid window i. The right hand side of Eq. (14) is the simplification of Shannon entropy of all sub-grids, in which DI^i can be considered as the average of logarithmic values of the variable distribution weighted by $\mu_j(L_\varepsilon)$ to quantify the degree of medium heterogeneity. Using Eq. (14), a series of values of DI^i (i=1,2,3…) are obtained for each measured cuboid window (Fig. 1b) of increment number i. For estimation of the REV in a porous medium, the relative increment of entropy dimension and associated criterion of REV identification are respectively expressed as:

$$RI^i = \left|\frac{DI^j - DI^{j-1}}{DI^{j-1}}\right| \times 100 = \left|\frac{DI^j - DI^{j-1}}{DI^{j-1}}\right| \times 100 \quad (15)$$

$$RI^i \leqslant 0.2CV_{DI} \quad (16)$$

where CV_{DI} is the coefficient of variation of DI^i series (i=1,2,3…), which is calculated through $CV_{DI} = (\hat{s}_{DI}/\overline{DI}) \times 100$; $\overline{DI}$ is the mean value of the DI^i series; $\hat{s}_{DI}$ is the standard deviation of the DI^i series.

To achieve the REV for multiple system variables, such as porosity, moisture saturation and air-water interfacial areas in an unsaturated porous medium, a criterion named the relative gradient error (Table 2) was applied (Costanza-Robinson et al., 2011):

$$\varepsilon_g^i = \left|\frac{\varphi^{i+1} - \varphi^{i-1}}{\varphi^{i+1} + \varphi^{i-1}}\right| \frac{1}{\Delta L} = \left|\frac{\varphi^{i+1} - \varphi^{i-1}}{\varphi^{i+1} + \varphi^{i-1}}\right| \frac{1}{\Delta L} \quad (17)$$

where ε_g^i is relative gradient error; ΔL is the measured cuboid window size increment

length for REV estimation. Usually, ε_g^i ~~ε_g^i~~ less than 0.2 (Costanza-Robinson et al., 2011) is utilized to identify a REV sizes.

According to the requirement in Eq. (12), a~~A~~ new criterion based on the required condition of REV is proposed to estimate the REV range for the translucent silica in this study:

$$\chi^i = \frac{|\delta^{i+1} - \delta^{i-1}|}{\delta^i \Delta L} \quad (18)$$

where δ^i ~~δ^i~~ is the dimensionless range, $\delta^i = \frac{\varphi(L_i)_{max} - \varphi(L_i)_{min}}{\overline{\varphi(L_i)}}$ ~~$\delta^i = \frac{\phi(L_i)_{\max} - \phi(L_i)_{\min}}{\overline{\phi(L_i)}}$~~; $\varphi(L_i)_{max}$ ~~$\varphi(L_i)_{max}$~~ is the maximum value of the variable on the volume scale L_i; $\varphi(L_i)_{min}$ ~~$\varphi(L_i)_{min}$~~ is the minimum value of the variable on the volume scale L_i; $\overline{\varphi(L_i)}$ ~~$\overline{\varphi(L_i)}$~~ is the mean value of the variable on the volume scale L_i. Brown and Hsieh (2000) suggested $\delta^i = \frac{\varphi(L_i)_{max} - \varphi(L_i)_{min}}{\overline{\varphi(L_i)}} << 1$ ~~$\delta^i = \frac{\phi(L_i)_{\max} - \phi(L_i)_{\min}}{\overline{\phi(L_i)}} << 1$~~ can be used for REV estimation. In fact, the calculated value of δ^i ~~δ^i~~ mostly is less than 1, while $\delta^i << 1$ ~~$\delta^i << 1$~~ is hard to be used to identify the REV scale for realistic materials, such as the translucent silica used in this study. The value limit of χ^i used for REV estimation also is explored in this study.

In this study, criteria for the coefficient of variation (C_V^i ~~C_V^i~~), entropy dimension (DI^i ~~DI^i~~), the relative gradient error (ε_g^i ~~ε_g^i~~) and the new criterion (χ^i) are all applied in REV estimation for porosity and PCE saturation. Corresponding REV plateau identification effects are compared to select the best criterion for REV quantification.

3. Results and discussion

3.1 REV identification effect of different criteria

3.1.1 The coefficient of variation

Emergent light intensity distributions of translucent silica for ~~two~~ three experiments, which had been fully saturated by water, was obtained by a thermoelectrically air-cooled ~~charge-coupled device (~~CCD~~)~~ camera (Niemet and Selker, 2001; Bob et al., 2008). The porosity, density, tortuosity and PCE saturation for ~~two~~ three experiments are derived by light transmission technique as shown in Figs. 3a and b. The PCE spreads from the injecting point shaped like a drop of water at t=~~1.44~~5 min (Fig. 3b). In 2D sandboxes for ~~two~~ three experiments, PCE plume infiltrates in translucent silica sands ~~infiltration paths~~ and ~~PCE plumes~~ reaches the bottom after t=80 min.

~~Every pixel with small scale could be approximated as infinitesimal element in high resolution image to apply light transmission techniques. As consequence, porosity of translucent silica was derived with light transmission technique through Eq. (5) (Fig. 2c). The whole 2D translucent silica area was numerically discretized that every cell had the uniform dimensions of 0.015m×0.015m. The cuboid window (Fig. 1bd) was utilized to quantify the variables (porosity, density, tortuosity, PCE saturation, PCE-water interfacial area) of every cell as measured scale was increased. In detail, the measured cuboid window scale was increased from the center of each cell and associated value of variable was calculated from the high resolution porosity of 2D translucent silica derived by light transmission technique. Observation cells were selected from the discretized cells (Fig. 3b) of which the cells I-1~2 and II-1~2 belong to Experiments I and II, respectively.~~ Porosity

292 and PCE saturation variation curves of ~~these~~ all observation cells with increasing measured
293 cuboid window scale were shown in Figs. 4a and b. However, for all observation cells from
294 translucent silica, the REV plateaus were not obvious to be objectively judged visually,
295 which made REV plateaus hard to identify effectively by original variation curves for
296 porosity and PCE saturation (Figs. 4a and b).

297 To make the REV plateau more explicit, different criteria of REV quantification are
298 utilized. The coefficient of variation (C_V^i ~~C_V^i~~) of porosity and PCE saturation fluctuating
299 with increase of measured cuboid window size is shown in Fig. 4. The measured cuboid
300 window scale is limited to the dimensions of cells in discretization of 2D translucent
301 silica. The observation cells show various characteristics of variation tendency for the
302 coefficient of variation (C_V^i ~~C_V^i~~). The θ and S_o variation curves of coefficient of variation
303 (C_V^i) for all observation cells do not reach stable values as those shown in Figs. 4a and b,
304 the beginning of the REV flat plateau is not easy to identify, the coefficient of variation (C_V^i
305 ~~C_V^i~~) is not suitable for REV estimation. According to the heterogeneity definition by
306 Corbett and Jensen (1992), the heterogeneity of materials is defined by C_V^i ~~C_V^i~~
307 magnitude that $0 < C_V^i < 0.5$ ~~$0 < C_V^i < 0.5$~~ is classed as homogeneous medium, $0.5 <$
308 $C_V^i < 1.0$ ~~$0.5 < C_V^i < 1.0$~~ is classed as heterogeneous medium and $1.0 < C_V^i$ ~~$1.0 < C_V^i$~~ is
309 classed as strong heterogeneous medium. For the coefficient of variation (C_V^i ~~C_V^i~~)
310 magnitude in Figs. 4a and b ~~f~~, the C_V^i ~~C_V^i~~ values are all below 0.5 that the criterion $C_V^i =$
311 0.5 ~~$C_V^i = 0.5$~~ is unable to identify the REV scale for translucent silica.

3.1.2 Entropy dimension

Entropy dimension (DI^i) is utilized by Martínez et al. (2007) for multifractal analysis of a porous medium porosity and REV estimation. In this study, entropy dimension (DI^i ~~DI^i~~) is tested to avoid unclear REV plateau in porosity curves. The entropy dimension (DI^i ~~DI^i~~) of porosity is calculated by Eq. (141). Variation curves of entropy dimension (DI^i ~~DI^i~~) for all observation cells (Fig. 2a) are presented in Fig. 4. The curves of entropy dimension (DI^i ~~DI^i~~) of porosity and PCE saturation generally result in the increasing trend curves which makes REV estimates become very difficult and invalid. Entropy dimension (DI^i ~~DI^i~~) was quickly increased with increasing of measured cuboid window size. Compared to the coefficient of variation (C_V^i ~~C_V^i~~) of porosity and PCE saturation, entropy dimension (DI^i ~~DI^i~~) increased step by step without opposite fluctuation tendency in the variation curves as length scale of measured cuboid window increased simultaneously. In general, REV plateau in region II (Fig. 1ae) of porosity is not obvious for the entropy dimension (DI^i ~~DI^i~~) curves of all observation cells from ~~two~~ three experiments, which suggests REV scales is uneasy to identify for translucent silica using entropy dimension (DI^i ~~DI^i~~) by light transmission technique.

3.1.3 The relative gradient error

The relative gradient error (ε_g^i ~~ε_g^i~~) of porosity and PCE saturation is calculated by Eq. (174). The variation of ε_g^i ~~ε_g^i~~ at different measured cuboid window scales are shown in Fig. 4 for all observation cells in the 2D translucent silica. For all ε_g^i ~~ε_g^i~~ curves at observation cells from experiments, the REV plateaus in region II (Fig. 1a) are more

clear than the variation curves based on the criteria of C_V^i ~~C_V^i~~ and DI^i ~~DI^i~~. Apparently, erratic variations of the relative gradient error (ε_g^i ~~ε_g^i~~) at small measured cuboid window scales are observed for all ε_g^i ~~ε_g^i~~ curves as the characteristic of REV region I in Fig. 1a~~e~~. When measured cuboid window scale further increases for all observation cells, the variability and magnitude of the relative gradient error (ε_g^i ~~ε_g^i~~) decrease well and factored into average, which can be identified as REV plateau in region II (Fig. 1a~~e~~). The relative gradient error (ε_g^i ~~ε_g^i~~) makes the REV plateau quantification convenient for all observation cells. At the measured cuboid window size above the REV plateau, ε_g^i ~~ε_g^i~~ curves result in large variability for observation cells I-1~2. These findings suggest that that the relative gradient error (ε_g^i ~~ε_g^i~~) can make the REV plateau more obvious, which greatly contribute to convenient and applicable REV quantification for translucent silica by light transmission technique. However, random fluctuations exist in ε_g^i ~~ε_g^i~~ curves visually, which make the REV plateau uneasy to identify accurately.

3.1.4 The new criterion (χ^i)

χ^i of porosity and PCE saturation changing with measured cuboid window size is shown in Fig. 4. Like the region I (Fig. 1a~~e~~), erratic and random fluctuations appears at small measured cuboid window sizes and χ^i increases with the increase of the measured cuboid window size. When measured scale increases, the values of χ^i for all observation cells appear fast reduction and rapidly tend to steady, which exhibit the characteristic of REV plateau as measured scale reaches region II. The χ^i for observation cells restore the erratic variation state of increasing trend after measured cuboid window size exceeding the REV plateau. As shown in the variation curves of χ^i for all observation cells, the beginning

of the REV flat plateaus can be identified easily, suggesting χ^i is more convenient and reliable than other methods for REV estimation. All observation cells show similar variation curves of χ^i that low value intervals are quite apparent, indicating that χ^i is very effective to make the REV plateau obvious for translucent silica used in this study. Using the criterion of χ^i, the REV plateau of region II is flat, which is easily identified, compared with other criteria for observation cells (Figs. 4a and b).

3.2 REVs of material properties

Based on the REV plateau identifications using the coefficient of variation (C_V^i ~~C_V^i~~),entropy dimension (DI^i ~~DI^i~~), the relative gradient error (ε_g^i ~~ε_g^i~~) and the proposed new criterion χ^i in Figs. 4a and b, the new criterion χ^i appears to be the most appropriate criterion for REV plateau identification. Even though the relative gradient error (ε_g^i ~~ε_g^i~~) can also make REV plateau obvious, but various random fluctuations weaken the method and reduce the associated accuracy. Therefore, REVs of porosity, density, tortuosity and PCE plume are estimated using the new criterion χ^i in the following study.

In fact, large number of discretized cells in the 2D translucent silica for ~~two~~ three experiments are quantified using the new criterion χ^i, which is convenient to examine the regularities for REV sizes and related factors. Using the new criterion χ^i, the REV estimation is conducted based on Eq. (1~~5~~8). Fig. 5a shows minimum REV sizes of porosity, density and tortuosity quantified by χ^i for all cells of ~~two~~ three experiments. Associated statistical analysis for REVs is illustrated in Fig. 5b, where circular points represent frequency and triangular points represent cumulative frequency. Frequency of REVs is dense in the middle and sparse on both sides, so the distribution of REVs can be fitted by Gaussian equation:

$$F = \omega + \frac{1}{\sqrt{2\pi\epsilon\varepsilon}} e^{-\frac{(REV-\nu)^2}{2\varepsilon\epsilon^2}} \quad (19)$$

where F is the frequency of REV; ω, ε ϵ and ν are fitted parameters of the model.

After regression analysis, the derived models for REV frequency are listed in Table 2. The coefficients of determination (R^2) of models for REVs of porosity and density for three experiments all exceed 0.85. R^2 for REV of tortuosity for three experiments exceed 0.76. Moreover, the computed cumulative frequency based on models fit cumulative frequency from experimental results well in Fig. 5b.

The minimum REV size frequency for porosity appears a peak between 4.0 mm and 5.0 mm for Experiment-I. As minimum REV size of porosity increases, corresponding frequency continuously decreases. Further, smooth convex shape of cumulative frequency is observed for minimum REV size of porosity (Fig. 5b). Most minimum REV sizes of translucent silica distributed in 0.0-7.0mm. For density of translucent silica sand, associated REV frequency appears high values between 2.0~3.0 mm. For the REV sizes of tortuosity, minimum REV sizes distribute in 0.0~6.0 mm. Compared with Experiment-I (F40/50 mesh translucent silica sand), the frequency of REV for Experiment-II (F20/30 mesh translucent silica sand with larger porosity) show flat shape and has larger value of standard deviation, especially for REV of porosity. Fig. 5b shows that translucent silica with larger porosity will achieve border distribution of minimum REV sizes distribution compared to translucent silica with relative lower porosity. Moreover, the frequency of REV of porosity and permeability for Experiment-III (background material is F20/30 mesh translucent silica sand with larger porosity, five lenses with lower porosity is packed in sandbox to create heterogeneity) is similar to the frequency of REV for Experiment-II. However, the

frequency of τ-REV for Experiment-III is different from the frequency of τ -REV for Experiment-II under homogeneous condition. The mean REV sizes of porosity, density and tortuosity for Experiment-I are 4.35 mm, 2.89 mm and 3.65 mm, respectively. All mean REV sizes of these variables for Experiment-II are larger than REVs of Experiments-I~~I~~, which corresponding mean REV sizes are 8.05 mm, 2.97 mm and 4.30 mm. These results suggest translucent porous media with higher porosity lead to larger values of mean and standard deviation for REV sizes.

3.3 REVs of S_o and A_{OW} for PCE plume

Based on the new criterion χ^i and light transmission technique, the real-time distributions of S_o-REV and A_{OW}-REV for PCE plume can be obtained over the entire experimental period. The minimum REV sizes of S_o and A_{OW} obtained using new criterion χ^i are shown in Figs. 6a and b.– When PCE migrates in sandbox, the REVs of PCE plume is changed over time (Fig. 6). The REVs of PCE plume for Experiment-I mostly are lower than the REVs of PCE plume for Experiments-II and III. Moreover, when heterogeneous porous media is packed in sandbox, the REV distribution of Experiment-III become more heterogeneous compared with REV distribution of Experiments-II under homogeneous condition. Based on REV distributions of PCE plume for three experiments, statistical analysis is conducted to explore the regularity of REV distribution for PCE plume. ~~To analyze the regularity of REV distribution for PCE plume, the mass center coordinate of PCE plume for two experiments are quantified for Experiments-I and II. The mass center coordinate are calculated as:~~

$$x_m = \frac{M_{10}}{M_{00}} \quad (17)$$

$$Z_m = \frac{M_{01}}{M_{00}} \quad (18)$$

where x_m is x coordinate of mass center for PCE plume; z_m is z coordinate of mass center for PCE plume; M_{00}, M_{10} and M_{01} are computed using definition of spatial moment (M_{ij}), $M_{ij} = \int_{x_0}^{x_1}\int_{z_0}^{z_1} \theta(x,z) S_o(x,z,t) x^i z^j d_x d_z$; x_0 and z_0 are minimum limits of x axis and z axis; x_1 and z_1 are maximum limits of x axis and z axis; θ(x,z) is the porosity at point (x,z); S_o(x,z,t) is PCE saturation of point (x, z) at time t.

The mass center coordinate of PCE plume, GTP and plume area derived by Eq. (18) are shown in Fig. 7a. The values of X_m, Z_m and GTP for Experiment-II and III are higher than the X_m, Z_m and GTP of Experiment-I (lower porosity). Moreover, the plume area of Experiment-II is larger than the plume of Experiment-I. When packed material is heterogeneous, the plume area of PCE is increased further for Experiment-III. Besides, the mean and standard deviation of REVs of PCE plume during 0~1523 min are derived by statistical analysis (Fig. 7a). Compared with REVs of PCE plume for Experiment-I, Experiment-II (F20/30 mesh translucent silica sand with higher porosity) has larger value of mean and standard deviation of REVs. The mean value of A_{OW}-REV for Experiment-III is much higher than A_{OW}-REV for Experiments-I and II.

Afterward, tThe average value of REVs ($\overline{REV}$ ~~$\overline{REV}$~~) and associated distance (d_m) from mass center to corresponding cells contained in PCE plume at t=1523 min are presented in Fig. 7ba. Regression analysis is performed for average REVs of PCE plume and d_m, where fitted models and associated R^2 for Experiments-I-III ~~and II~~ are listed in Table 43.

Simultaneously, the fitted equations between $\overline{REV}$ ~~$\overline{REV}$~~ and d_I (the distance from injection point to cell contained in PCE plume) also are derived by regression analysis. From the results in Fig. 7a, $\overline{REV}$ ~~$\overline{REV}$~~ of S_o and A_{ow} appear a peak and then decrease with increasing of d_m and d_I for Experiment-I. $\overline{REV}$ ~~$\overline{REV}$~~ of S_o and A_{ow} for Experiment-I all firstly increase and then decrease with the increasing of d_m and d_I~~,~~. However~~while~~, ~~$\overline{REV}$~~ $\overline{REV}$ of ~~PCE plume~~S_o presents apparent decreasing tendency as d_m and d_I increase for Experiment-II, and $\overline{REV}$ of A_{ow} just slightly increase first and then decrease for Experiment-II. In addition, the value of A_{OW}-REV mostly is higher than the value of S_o-REV for ~~two~~ three experiments. Compared with the R^2 of the fitted relationship between average REVs of PCE plume and d_m, d_I for Experiments-I and II, the values of R^2 achieved by Experiment-III are much lower (Table 3).

~~The mean and standard deviation of REVs of PCE plume during 0~1523 min derived by statistical analysis (Fig. 7b). Compared with REVs of PCE plume for Experiment-I, Experiment-II (F20/30 mesh translucent silica sand with higher porosity) has larger value of mean and standard deviation of REVs.~~ Besides, the relationship between REVs and PCE saturation are fitted by regression analysis, where fitted equation and R^2 for ~~two~~ three experiments are listed in Table 4~~5~~ and Fig. 7b. With increasing of PCE saturation, REV of S_o appear decline trend for ~~two~~ three experiments. However, REV of A_{OW} increases when S_o increases for ~~both two~~all three experiments (Fig. 7b). On the other hand, REV of S_o for Experiment-II is higher than corresponding REV for Experiment-I, while Experiments-I and II have similar values of A_{OW}-REV (Fig. 7b). Moreover, REVs of S_o and A_{OW} for Experiment-III are higher than REVs of S_o and A_{OW} for Experiments-I and II. These results

suggest higher porosity will lead to high value of S_o-REV and the relationship between REVs of PCE plume and dm, d_l. S_o-REV and A_{OW}-REV are increased under heterogeneous condition.

4. Conclusions

In this study, a new criterion χ^i is proposed to identify the REVs of translucent porous media and inner contaminant transformation based on previous criteria. The REV plateaus of observation cells selected from ~~two~~ three experiments of PCE transport are hard to judge visually from the porosity and PCE saturation curves. From the REV identification effects of different criteria, the REV flat plateau is difficult to identify by coefficient of variation (C_V^i ~~C_V^i~~) and entropy dimension (DI^i ~~DI^i~~), indicting the coefficient of variation (C_V^i ~~C_V^i~~) and entropy dimension (DI^i ~~DI^i~~) are not suitable for REV estimation of translucent porous media. The relative gradient error (ε_g^i ~~ε_g^i~~) can make REV plateaus of all kinds of translucent silica explicit in variation curves, but random fluctuations weaken REV plateau identification. In comparison with these previous criteria, the beginning and ending of the REV flat plateaus could be easily and directly identified in the curves based on the new criterion χ^i, suggesting the new criterion χ^i is more convenient and effective for REV estimation. In this study, REVs of porosity, density, tortuosity, and PCE plume are estimated using the new criterion χ^i.

Statistical results of minimum REV scales quantified by new criterion χ^i reveal cumulative frequencies of porosity, density and tortuosity all have smooth convex shapes. Models based on Gaussian equation are built for the distribution of REVs of porosity, density and tortuosity, which porous media with larger porosity leads to larger values of

mean and standard deviation for REV sizes of media properties. For REVs of PCE plume, result suggested larger porosity lead to larger value of mean and standard deviation. Regression analysis is performed to study the regularity for distribution of REVs, where fitted relationship between REVs and d_m, d_l are derived for PCE plume. ~~REV~~ of S_o and A_{ow} firstly increase and then decrease with the increasing of d_m and d_l for Experiment-I whose sandbox packed by translucent porous media with relatively lower porosity. However, ~~REV~~ of S_o and A_{ow} directly decrease with the increment of d_m and d_l when porosity became larger for Experiment-II. The values of R^2 of the fitted relationship between average REVs of PCE plume and d_m, d_l for Experiment-III are much lower under heterogeneous condition. Significantly, REV size of S_o presented decreasing trend as S_o increases, while increasing tendency appeared for REV size of A_{ow}. Through regression analysis, the fitted equations between REVs of PCE plume and PCE saturation are derived for ~~two~~ three experiments. Implications of these finding are essential for quantitative investigation of scale effect of porous media and contaminant transformation. The fluid migration and transform in porous media can be simulated accurately according to the REV estimation results using light transmission technique and the appropriate criterion χ^i.

Code and data availability

The codes and data for this paper are available by contacting the corresponding author at jfwu@nju.edu.cn.

Author contributions

Ming Wu: Conceptualization, Methodology, Writing;

Jianfeng Wu: Conceptualization, Methodology, Writing;

Jichun Wu: Conceptualization;

Bill X. Hu: Conceptualization, Writing.

Declaration of interests

The authors declare that they have no known competing financial interests or personal relationships that could have appeared to influence the work reported in this paper.

Acknowledgments

We acknowledge support by the National Key Research and Development Plan of China (2019YFC1805302 and 2016YFC0402800), the National Natural Science Foundation of China (41902246, 41730856 and 41772254), the Natural Science Foundation of Guangdong Province (2020A1515010447) and, the Fundamental Research Funds for the Central Universities (14380105)the National Natural Science Foundation of China-Xianjiang Project (U1503282) and the China Postdoctoral Science Foundation (2017M622905).

References

Al-Raoush, R., and Papadopoulos, A.: Representative elementary volume analysis of porous media using X-ray computed tomography, Power Technol., 200, 60-77, 2010.

523 Al-Raoush, R.: Change in Microstructure Parameters of Porous Media Over Representative
524 Elementary Volume for Porosity, Part. Sci. Technol., 30, 1-16, 2012.
525 Bai, L., Wang, X., Chen, Q., Ye, Y., Zheng, H., Guo, J., Yin, Y., and Gao, C.: Explaining the
526 Size Dependence in Platinum-Nanoparticle-Catalyzed Hydrogenation Reactions,
527 Angew. Chem. Int. Ed., 55, 15656-15661, 2016.
528 Bob, M.M., Brooks, M.C., Mravik, S.C., and Wood, A.L.: A modified light transmission
529 visualization method for DNAPL saturation measurements in 2-D models, Adv.
530 Water Resour., 31, 727-742, 2008.
531 Borges, J.A.R., and Pires, L.F.: Representative elementary area (REA) in soil bulk density
532 measurements through gamma ray computed tomography, Soil Till. Res., 123, 43-
533 49, 2012.
534 Borges, JAR., Pires, L.F., Cássaro, F.A.M., Roque, W.L., Heck, R.J., Rosa, J.A., and Wolf,
535 F.G.: X-ray microtomography analysis of representative elementary volume (REV)
536 of soil morphological and geometrical properties, Soil Till. Res., 182, 112-122,
537 2018.
538 Bouvry, B., del Campo, L., Meneses, D.D.S., Rozenbaum, O., Echegut, R., Lechevalier, D.,
539 Gaubil, M., and Echegut, P.: Hybrid methodology for retrieving thermal radiative
540 properties of semi-transparent ceramics, J. Phys. Chem. C, 120, 3267-3274, 2016.
541 Bradford, S.A., Vendlinski, R.A., and Abriola, L.M.: The entrapment and long-term
542 dissolution of tetrachloroethylene in fractional wettability porous media, Water
543 Resour. Res., 35(10), 295-2964, 1999.
544 Brown, G.O., and Hsieh, H.T.: Evaluation of laboratory dolomite core sample size using

545 representative elementary volume concepts, Water Resour. Res., 36(5), 1199-1207,
546 2000.
547 Corbett, P.W.M., and Jensen, J.L.: Estimating the mean permeability: how many
548 measurement do we need? First Break, 10(3), 89-94, 1992.
549 Costanza-Robinson, M.S., Estabrook, B.D., and Fouhey, D.F.: Representative elementary
550 volume estimation for porosity, moisture saturation, and air-water interfacial areas
551 in unsaturated porous media: Data quality implication, Water Resour. Res., 47,
552 W07513, 2011.
553 Erning, K., Grandel, S., Dahmke, A., and Schäfe, D.: Simulation of DNAPL infiltration and
554 spreading behavior in the saturated zone at varying flow velocities and alternating
555 subsurface geometries, Environ. Earth Sci., 65, 1119-1131, 2012.
556 Esfandiar, A., Radha, B., Wang, F.C., Yang, Q., Hu, S., Garaj, S., Nair, R.R., Geim, A.K.,
557 and Gopinadhan, K.: Size effect in ion transport through angstrom-scale slits,
558 Science, 358, 511-513, 2017.
559 Fernandes, J.S., Appoloni, C.R., and Fernandes, C.P.: Determination of the Representative
560 Elementary Volume for the study of sandstones and siltstones by X-Ray
561 microtomography, Mater. Res., 15(4), 662-670, 2012.
562 Ghilardi, P., Kai, A.K., and Menduni, G.: Self-similar heterogeneity in granular porous
563 media at the representative elementary volume scale, Water Resour. Res., 29(4),
564 1205-1214, 1993.
565 Gilevska, T., Passeport, E., Shayan, M., Seger, E., Lutz, E.J., West, K.A., Morgan, S.A.,
566 Mack, E.E., and Lollar, B.S.: Determination of in situ biodegradation rates via a

567 novel high resolution isotopic approach in contaminated sediments, Water Res, 149,
568 632-639, 2019.
569 Hendrick, A.G., Erdmann, R.G., and Goodman, M.R.: Practical Considerations for
570 Selection of Representative Elementary Volumes for Fluid Permeability in Fibrous
571 Porous Media, Transp. Porous Med., 95, 389-405, 2012.
572 Kang, Q.J., Zhang, D.X., and Chen, S.Y.: Simulation of dissolution and precipitation in
573 porous media, J. Geophys. Res. 108, NO. B10, 2505, doi:10.1029/2003JB002504,
574 2003.
575 Kim, J., and Mohanty, B.P.: Influence of lateral subsurface flow and connectivity on soil
576 water storage in land surface modeling, J. Geophys. Res. Atmos., 121,704-721,
577 2016.
578 Lei, S., and Shi, Y.: Separate-phase model and its lattice Boltzmann algorithm for liquid-
579 vapor two-phase flows in porous media, Phys. Rev. E, 99, 053302, 2019.
580 Martínez, F.S.J., Caniego, F.J., García-Gutiérrez, C., and Espejo, R.: Representative
581 elementary area for multifractal analysis of soil porosity using entropy dimension,
582 Nonlin. Processes Geophys., 14, 503-511, 2007.
583 Müller, C., and Siegesmund, S.: Evaluation of the representative elementary volume (REV)
584 of a fractured geothermal sandstone reservoir, Environ. Earth Sci., 61, 1713-1724,
585 2010.
586 Niemet, M.R., and Selker, J.S.: A new method for quantification of liquid saturation in 2D
587 translucent porous media systems using light transmission, Adv. Water Resour., 24,
588 651-666, 2001.

589 Nordahl, K., and Ringrose, P.S.: Identifying the Representative Elementary Volume for
590 permeability in heterolithic deposits using numerical rock models, Math Geosci.,
591 40, 753-771, 2008.
592 O'Carroll, D.M., Bradford, S.A., and Abriola, L.M.: Infiltration of PCE in a system
593 containing spatial wettability variations, J. Contam. Hydrol., 73, 39-63, 2004.
594 Pereira Nunes, J.P., Blunt, M.J., and Bijeljic, B.: Pore-scale simulation of carbonate
595 dissolution in micro-CT images, J. Geophys. Res. Solid Earth, 121, 558-576, 2016.
596 Piccoli, I, Schjønning, P., Lamandé, M., Zanini, F., and Morari, F.: Coupling gas transport
597 measurements and X-ray tomography scans for multiscale analysis in silty soils,
598 Geoderma, 338, 576-584, 2019.
599 Razavi, M.R., Muhunthan, B., and Al Hattamleh, O.: Representative elementary volume
600 analysis of sands using x-ray computed tomography, Geotech. Test J., 30(3), 212-
601 219, 2007.
602 Rozenbaum, O., and du Roscoat, S.R.: Representative elementary volume assessment of
603 three-dimensional x-ray microtomography images of heterogeneous
604 materials:Application to limestones, Phys. Rev. E, 89, 053304, 2014.
605 Teruel, F.E., and Rizwan-uddin: Numerical computation of macroscopic turbulence
606 quantities in representative elementary volumes of the porous medium, Int. J. Heat
607 Mass Transfer., 53, 5190-5198, 2010.
608 Ukrainczyk, N., and Koenders, E.A.B.: Representative elementary volumes for 3D
609 modeling of mass transport in cementitious materials, Modelling Simul. Mater. Sci.
610 Eng., 22, 035001, 2014.

611 Wang, L., Mi, J., and Guo, Z.: A modified lattice Bhatnagar–Gross–Krook model for
612 convection heat transfer in porous media, Int. J. Heat Mass Transfer., 94, 269-291,
613 2016.
614 Wang, S., Elsworth, D., and Liu, J.: A mechanistic model for permeability evolution in
615 fractured sorbing media, J. Geophys. Res, 117, B06205,
616 doi:10.1029/2011JB008855, 2012.
617 Wu, M., Wu, J.F., and Wu, J.C.: Simulation of DNAPL migration in heterogeneous
618 translucent porous media based on estimation of representative elementary volume,
619 J. Hydrol., 553, 276-288, 2017.
620 Wu, M., Wu, J.F., Wu, J.C., and Hu, B.X.: Effects of microarrangement of solid particles on
621 PCE migration and its remediation in porous media, Hydrol. Earth Syst. Sci., 22,
622 1001-1015, 2018.
623

Table 1. Experimental conditions

Experiment	I	II	III
Sandbox dimensions (cm)	20×15	60×45	60×45
~~Packed translucent silica sand~~Background translucent silica sand	F40/50	F20/30	F20/30
Medium condition	Homogeneity	Homogeneity	Heterogeneity
Median grain diameter (mm)	0.36	0.72	0.72
Permeability (m^2)	4.25×10^{-11}	1.35×10^{-10}	1.35×10^{-10}
V_{PCE} (ml)	9	32	40
Injection rate (ml/min)	0.5	0.5	0.5

627 **Table 2.** Criteria of REV estimation

Criterion	Equation
The coefficient of variation	$C_V^i = \frac{\hat{s}}{\overline{\varphi}_i}$
entropy dimension	$DI^i \approx \frac{\sum_{j=1}^{m(i)} \mu_j(L_\varepsilon) \log \mu_j(L_\varepsilon)}{\log L_\varepsilon}$
the relative gradient error	$\varepsilon_g^i = \left\| \frac{\varphi^{i+1} - \varphi^{i-1}}{\varphi^{i+1} + \varphi^{i-1}} \right\| \frac{1}{\Delta L}$
New criterion	$\chi^i = \frac{\lvert \delta_{i+1} - \delta_{i-1} \rvert}{\delta_i \Delta L}$

628

629

Table 23. The fitted equations of frequency for REVs of porosity, density and tortuosity

Experiment	I	II
θ-REV	$F = -2.01\times10^{-12} + \frac{1}{\sqrt{2\pi}\times1.50}e^{-\frac{(REV-4.35)^2}{2*1.50^2}}$ (R^2=0.955)	$F = -5.30\times10^{-3} + \frac{1}{\sqrt{2\pi}\times3.35}e^{-\frac{(REV-8.05)^2}{2*3.35^2}}$ (R^2=0.932)
ρ-REV	$F = -7.51\times10^{-26} + \frac{1}{\sqrt{2\pi}\times1.14}e^{-\frac{(REV-2.89)^2}{2*1.14^2}}$ (R^2=0.969)	$F = -3.18\times10^{-12} + \frac{1}{\sqrt{2\pi}\times1.71}e^{-\frac{(REV-2.97)^2}{2*1.71^2}}$ (R^2=0.989)
τ-REV	$F = -2.76\times10^{-15} + \frac{1}{\sqrt{2\pi}\times1.42}e^{-\frac{(REV-3.65)^2}{2*1.42^2}}$ (R^2=0.774)	$F = -8.55\times10^{-8} + \frac{1}{\sqrt{2\pi}\times2.15}e^{-\frac{(REV-4.30)^2}{2*2.15^2}}$ (R^2=0.850)

*F represents the frequency of REV, θ represents porosity, ρ represents density, τ represents tortuosity

Experiment		I	II	III
θ-REV	ω	-2.11×10^{-4}	-1.45×10^{-3}	7.63×10^{-4}
	ϵ	1.73	3.45	3.18
	ν	4.35	7.90	6.50
	R^2	0.938	0.924	0.907
ρ-REV	ω	-6.51×10^{-4}	-2.51×10^{-4}	1.51×10^{-3}
	ϵ	1.08	1.66	2.40
	ν	2.89	2.97	3.70
	R^2	0.967	0.990	0.859
τ-REV	ω	-3.36×10^{-4}	-2.04×10^{-4}	1.29×10^{-3}
	ϵ	1.39	2.15	1.20
	ν	3.65	4.20	1.05
	R^2	0.769	0.875	0.919

*θ represents porosity, ρ represents density, τ represents tortuosity; ω, ϵ and ν are fitted parameters of the model

637 **Table 34.** The fitted equations between average value of REV and d_I, d_m

Experiment		I		II	
		S_o-REV	A_{OW}-REV	S_o-REV	A_{OW}-REV
d_m		$\overline{REV} = -1.67\times10^{-3}d_m^2 + 0.193d_m + 2.72$ (R^2=0.807)	$\overline{REV} = -6.10\times10^{-4}d_m^2 + 5.82\times10^{-2}d_m + 7.20$ (R^2=0.401)	$\overline{REV} = -4.08\times10^{-5}d_m^2 + 1.50\times10^{-2}d_m + 7.54$ (R^2=0.655)	$\overline{REV} = -1.92\times10^{-5}d_m^2 + 4.47\times10^{-3}d_m + 9.46$ (R^2=0.616)
d_I		$\overline{REV} = -1.97\times10^{-3}d_I^2 + 0.245d_I + 1.12$ (R^2=0.832)	$\overline{REV} = -1.47\times10^{-3}d_I^2 + 0.205d_I + 1.84$ (R^2=0.733)	$\overline{REV} = -3.94\times10^{-5}d_I^2 + 7.80\times10^{-3}d_I + 8.50$ (R^2=0.327)	$\overline{REV} = -1.92\times10^{-5}d_m^2 + 4.47\times10^{-3}d_m + 9.46$ (R^2=0.616)

638

Experiment		d_m	d_I
I	S_o-REV	$\overline{REV} = -1.67\times10^{-3}d_m^2 + 0.193d_m + 2.72$ (R^2=0.807)	$\overline{REV} = -1.97\times10^{-3}d_I^2 + 0.245d_I + 1.12$ (R^2=0.832)
	A_{OW}-REV	$\overline{REV} = -6.10\times10^{-4}d_m^2 + 5.82\times10^{-2}d_m + 7.20$ (R^2=0.401)	$\overline{REV} = -1.47\times10^{-3}d_I^2 + 0.205d_I + 1.84$ (R^2=0.733)
II	S_o-REV	$\overline{REV} = -4.08\times10^{-5}d_m^2 + 1.50\times10^{-2}d_m + 7.54$ (R^2=0.655)	$\overline{REV} = -3.94\times10^{-5}d_I^2 + 7.80\times10^{-3}d_I + 8.50$ (R^2=0.327)
	A_{OW}-REV	$\overline{REV} = -1.92\times10^{-5}d_m^2 + 4.47\times10^{-3}d_m + 9.46$ (R^2=0.616)	$\overline{REV} = -1.92\times10^{-5}d_I^2 + 4.47\times10^{-3}d_I + 9.46$ (R^2=0.616)
III	S_o-REV	$\overline{REV} = -6.06\times10^{-6}d_m^2 + 2.27\times10^{-3}d_m + 7.76$ (R^2=0.153)	$\overline{REV} = 1.69\times10^{-5}d_I^2 - 1.21\times10^{-2}d_I + 9.62$ (R^2=0.236)
	A_{OW}-REV	$\overline{REV} = -8.71\times10^{-6}d_m^2 + 5.66\times10^{-3}d_m + 11.5$ (R^2=0.115)	$\overline{REV} = -1.50\times10^{-5}d_I^2 + 7.88\times10^{-3}d_I + 11.4$ (R^2=0.150)

639

640 * ~~$\overline{REV}$~~ $\overline{REV}$ is the average value of REV size, d_m is the distance from mass center of PCE

641 plume to the cell contained in PCE plume, d_I is the distance from injection point to the cell
642 contained in PCE plume
643
644

Table 4~~5~~. The fitted relationship between REV and S_o

~~Experiment~~	~~I~~	~~II~~
~~S_o-REV~~	~~$REV = -2.13 \times \ln S_o + 0.876$~~ ~~($R^2$=0.466)~~	~~$REV = -0.961 \times \ln S_o + 1.09$~~ ~~($R^2$=0.415)~~
~~A_{OW}-REV~~	~~$REV = 2.27e^{2.70*S_o}$~~ ~~(R^2=0.366)~~	~~$REV = 1.70e^{3.30*S_o}$~~ ~~(R^2=0.500)~~

Experiment	S_o-REV	A_{OW}-REV
I	$REV = -2.13 \times \ln S_o + 0.876$ (R^2=0.466)	$REV = 2.27e^{2.70 \times S_o}$ (R^2=0.366)
II	$REV = -0.961 \times \ln S_o + 1.09$ (R^2=0.415)	$REV = 1.70e^{3.30 \times S_o}$ (R^2=0.500)
III	$REV = -1.40 \times \ln S_o + 3.96$ (R^2=0.538)	$REV = 2.05e^{3.22 \times S_o}$ (R^2=0.573)

Figure Captions

Figure 1. ~~(a) System Device for acquisition of properties of translucent material; (b) The infinitesimal selected from translucent porous media packed in 2D sandbox;~~ (a~~c~~) Variable changes as measured scale (L) increment in conceptual curve (Costanza-Robinson et al., 2011); (b~~d~~) Scale effect and the cuboid image window geometry; (c) System Device for acquisition of parameters (porosity and density, etc.) of translucent material; (d) The infinitesimal selected from translucent porous media packed in 2D sandbox.

Figure 2. (a) The system sandbox equipment of Experiment-I; (b) The system sandbox equipment of Experiment-II; (c) The system sandbox equipment of Experiment-III

Figure 3. (a) The emergent light intensity, porosity, permeability and tortuosity of 2D translucent silica sand for Experiments-I-III ~~and II~~; (b) The PCE saturation of Experiments-I-III ~~and II~~ during 0~1523 min and observation cells

Figure 4. (a) The change of porosity (θ), associated coefficient of variation (C_V^i ~~C_V^i~~), entropy dimension (DI^i ~~DI^i~~), the relative gradient error (ε_g^i ~~ε_g^i~~), and new criterion-χ^i for observation cells as cuboid window scale (L) increases; (b) The change of PCE saturation (S_o), associated C_V^i ~~C_V^i~~, DI^i ~~DI^i~~, ε_g^i ~~ε_g^i~~, and χ^i for observation cells as cuboid window scale (L) increases

Figure 5. (a) The distributions of minimum REV sizes of porosity, sand density and tortuosity for Experiments-I-III ~~and II~~; (b) The frequency of minimum REV sizes of Experiments and fitted models

Figure 6. (a) The distributions of S_o-REV sizes during 0~1523 min for Experiments-I-III

~~and II~~; (b) The distributions of A_{OW}-REV sizes during 0~1523 min for Experiments-I-III ~~and II~~

Figure 7. (a) The mass center coordinate of PCE plume, GTP, plume area and the mean, standard deviation of S_o-REV and A_{OW}-REV during 0~1523 min~~The mass center coordinate of PCE plume and the change of average REV size as the distance d_I, d_m increases~~; (b) ~~The mean, standard deviation of S_o-REV and A_{OW}-REV during 0~1523 min~~ The change of average REV size as the distance d_I, d_m increases and fitted relationship between REV sizes and S_o for Experiments-I and II

682 **Fig. 1**

683

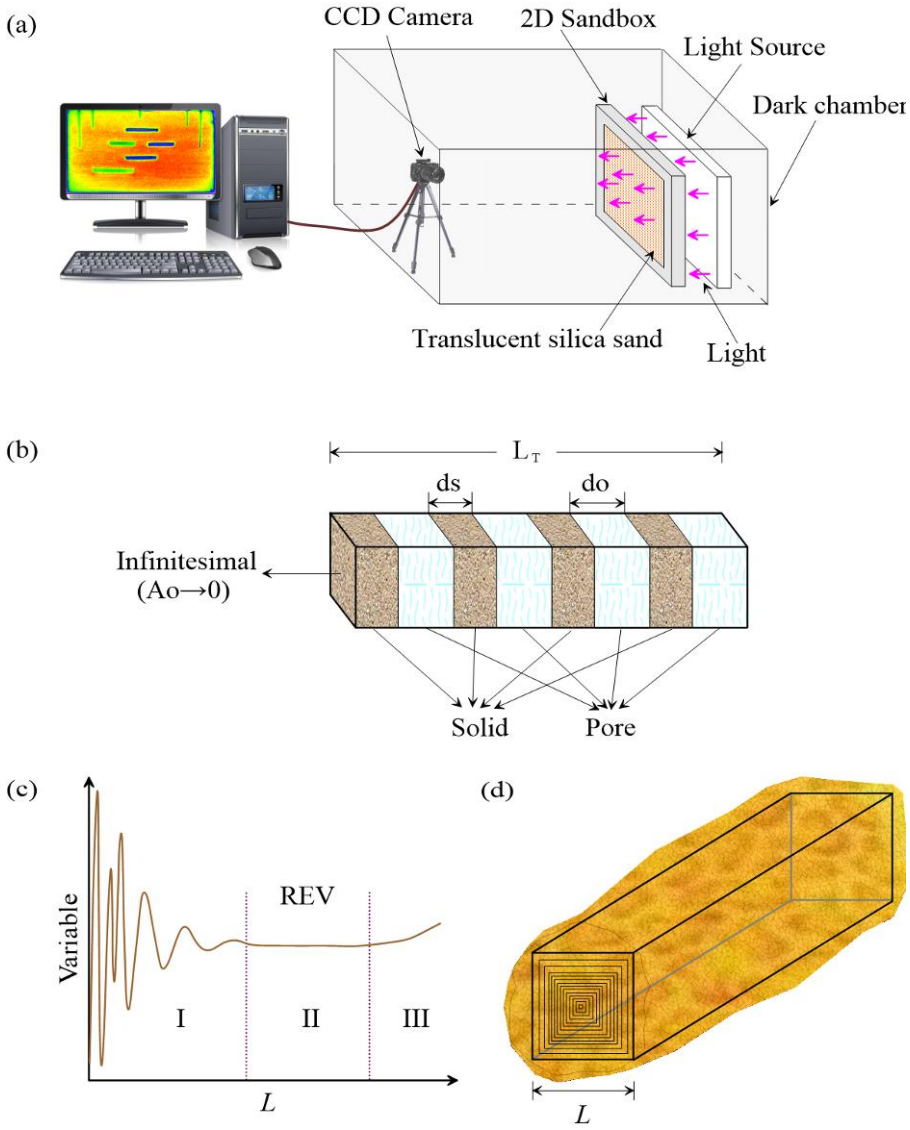

684

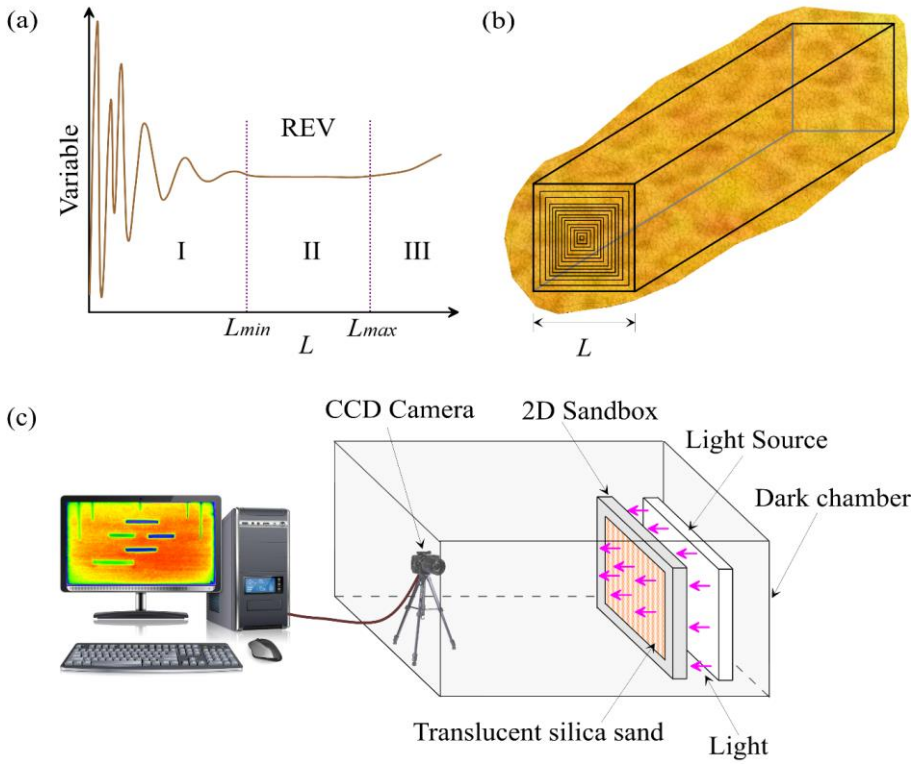
(a)
Variable
REV
I
II
III
Lmin
L
Lmax
(b)
L
(c)
CCD Camera
2D Sandbox
Light Source
Dark chamber
Translucent silica sand
Light
(d)
L_T
ds
do
Infinitesimal
(Ao→0)
Solid
Pore

685

686

687 **Fig. 2**

688

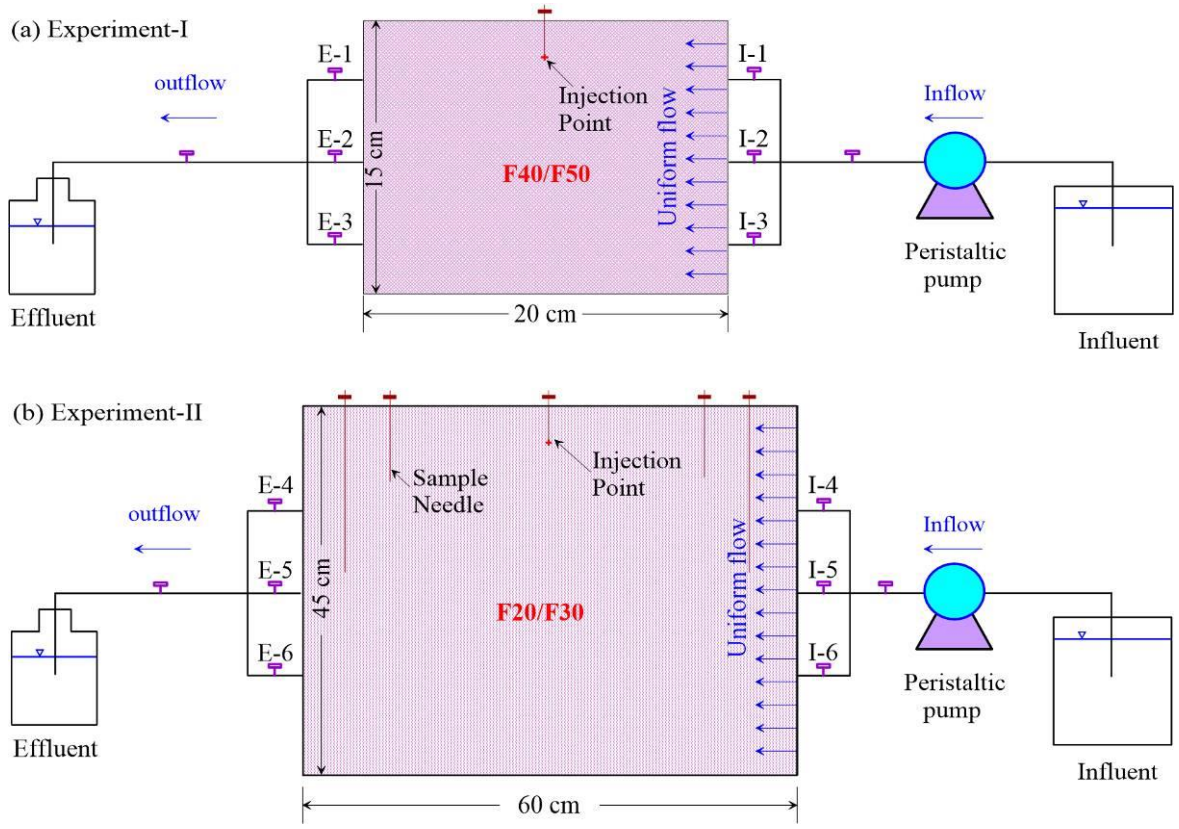

689

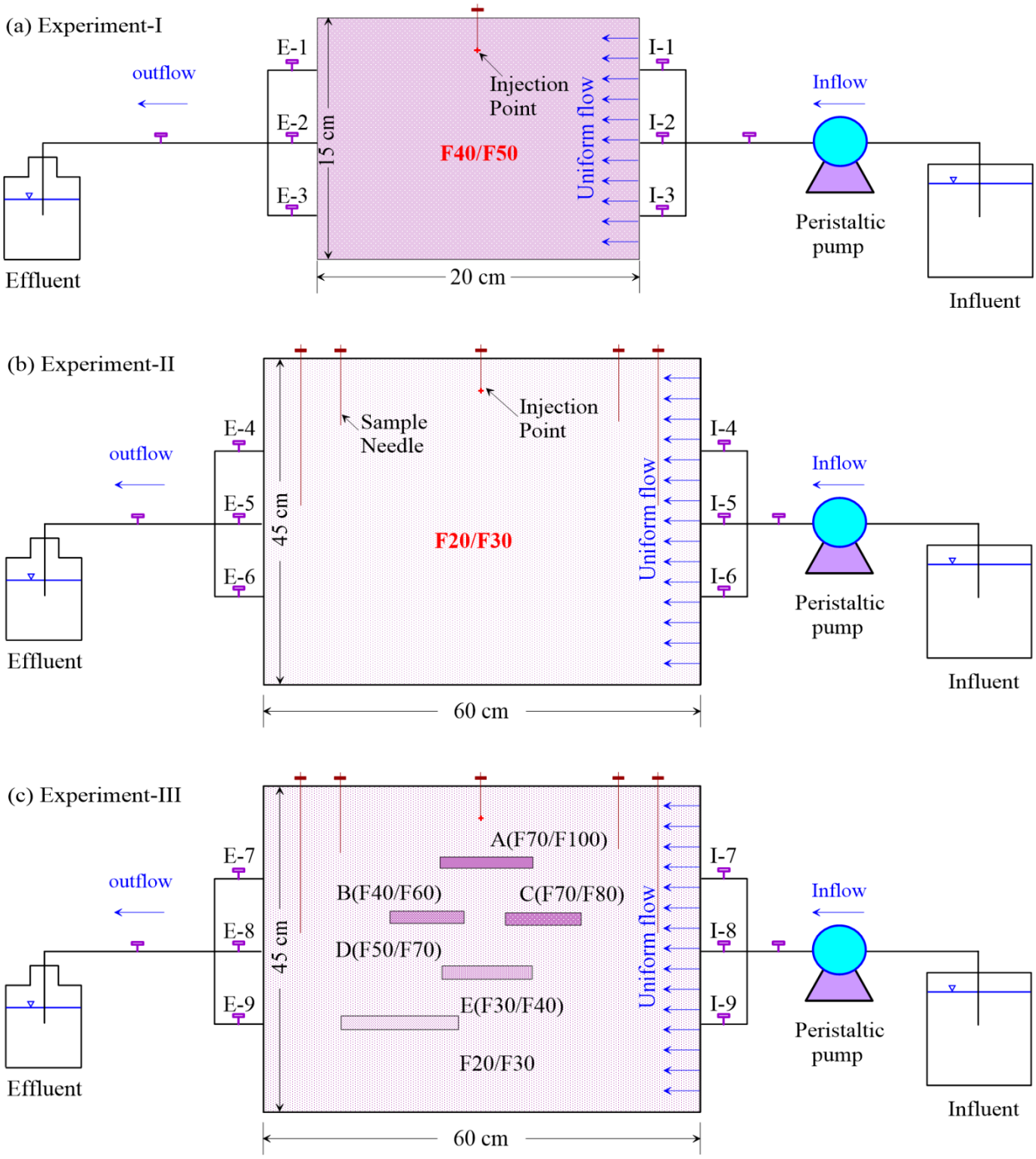
(a) Experiment-I
outflow
E-1
E-2
E-3
15 cm
Injection Point
F40/F50
Uniform flow
I-1
I-2
I-3
Inflow
Peristaltic pump
Effluent
20 cm
Influent
(b) Experiment-II
Sample Needle
Injection Point
E-4
E-5
E-6
45 cm
F20/F30
Uniform flow
I-4
I-5
I-6
outflow
Inflow
Peristaltic pump
Effluent
60 cm
Influent
(c) Experiment-III
A(F70/F100)
B(F40/F60)
C(F70/F80)
D(F50/F70)
E(F30/F40)
F20/F30
E-7
E-8
E-9
45 cm
Uniform flow
I-7
I-8
I-9
outflow
Inflow
Peristaltic pump
Effluent
60 cm
Influent

Fig. 3

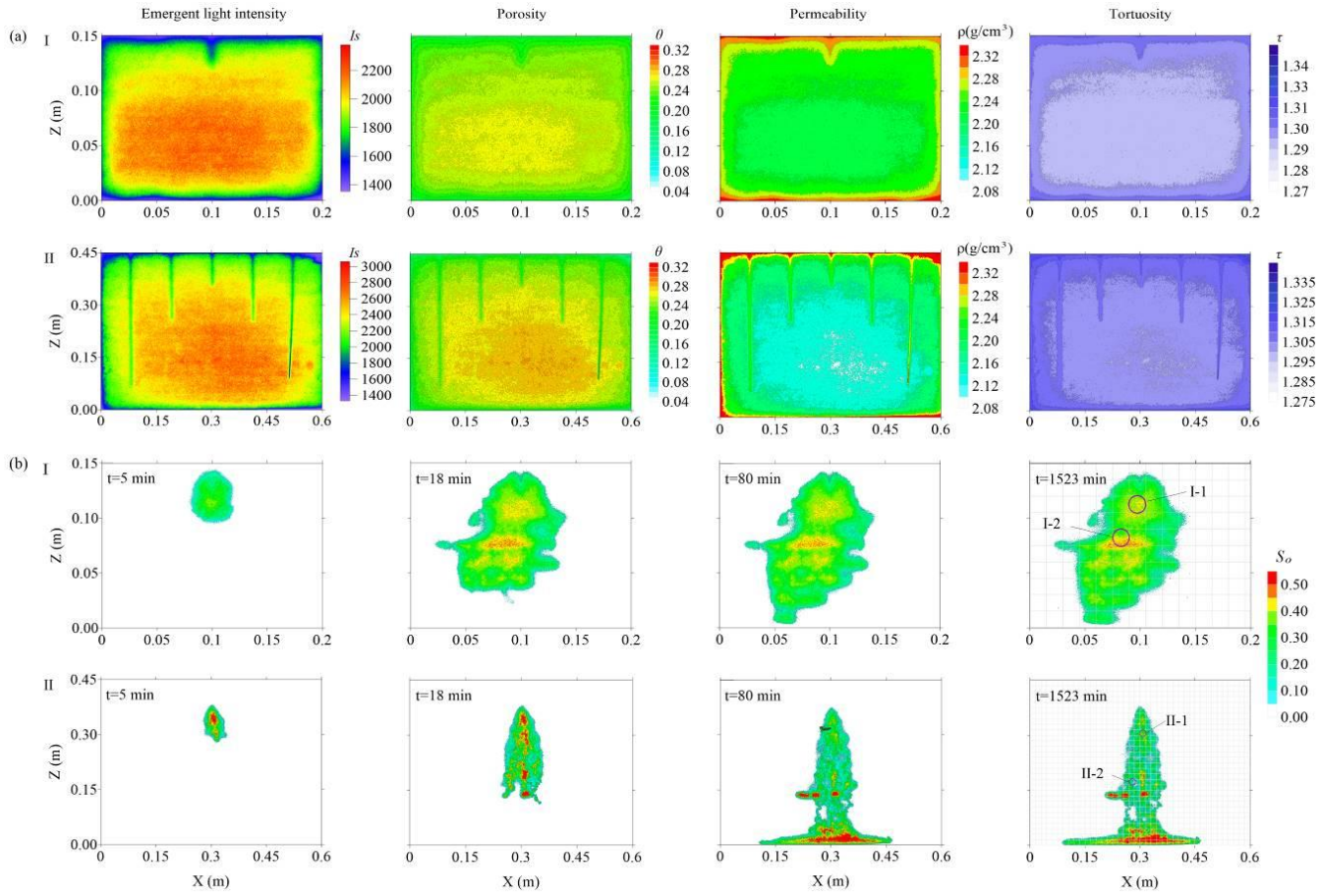
Emergent light intensity
Porosity
Permeability
Tortuosity
(a)
I
II
Z (m)
Is
θ
ρ(g/cm³)
τ
(b)
t=5 min
t=18 min
t=80 min
t=1523 min
I-1
I-2
II-1
II-2
So
X (m)

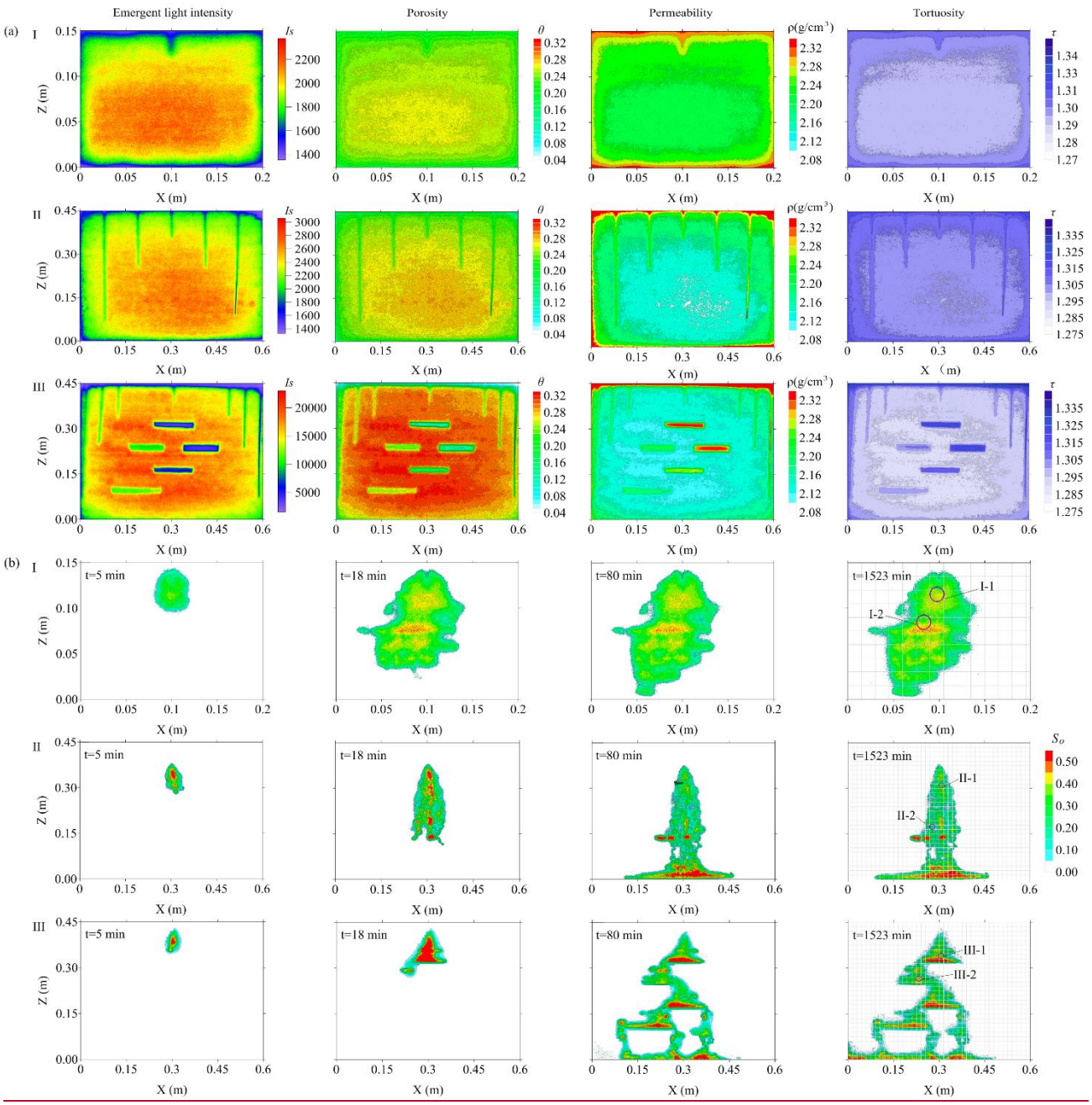
(a)
Emergent light intensity
Porosity
Permeability
Tortuosity
I
II
III
Z (m)
X (m)
Is
θ
ρ(g/cm³)
τ
(b)
t=5 min
t=18 min
t=80 min
t=1523 min
I-1
I-2
II-1
II-2
III-1
III-2
So

695

Fig. 4

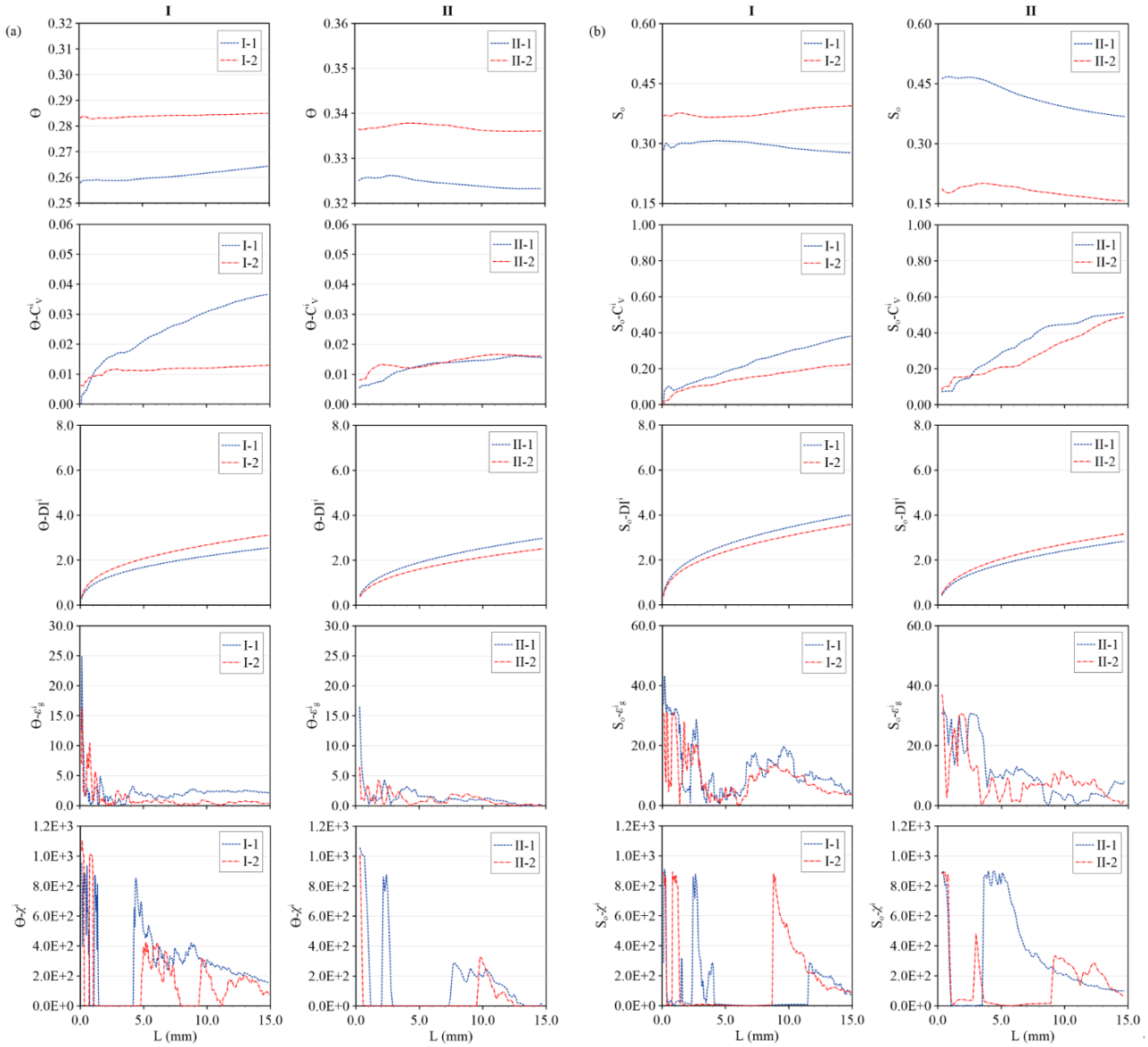
(a)
(b)
I
II
I-1
I-2
II-1
II-2
Θ
S_δ
Θ-C_V^i
S_δ-C_V^i
Θ-DI^i
S_δ-DI^i
Θ-ε_g^i
S_δ-ε_g^i
Θ-χ^i
S_δ-χ^i
L (mm)

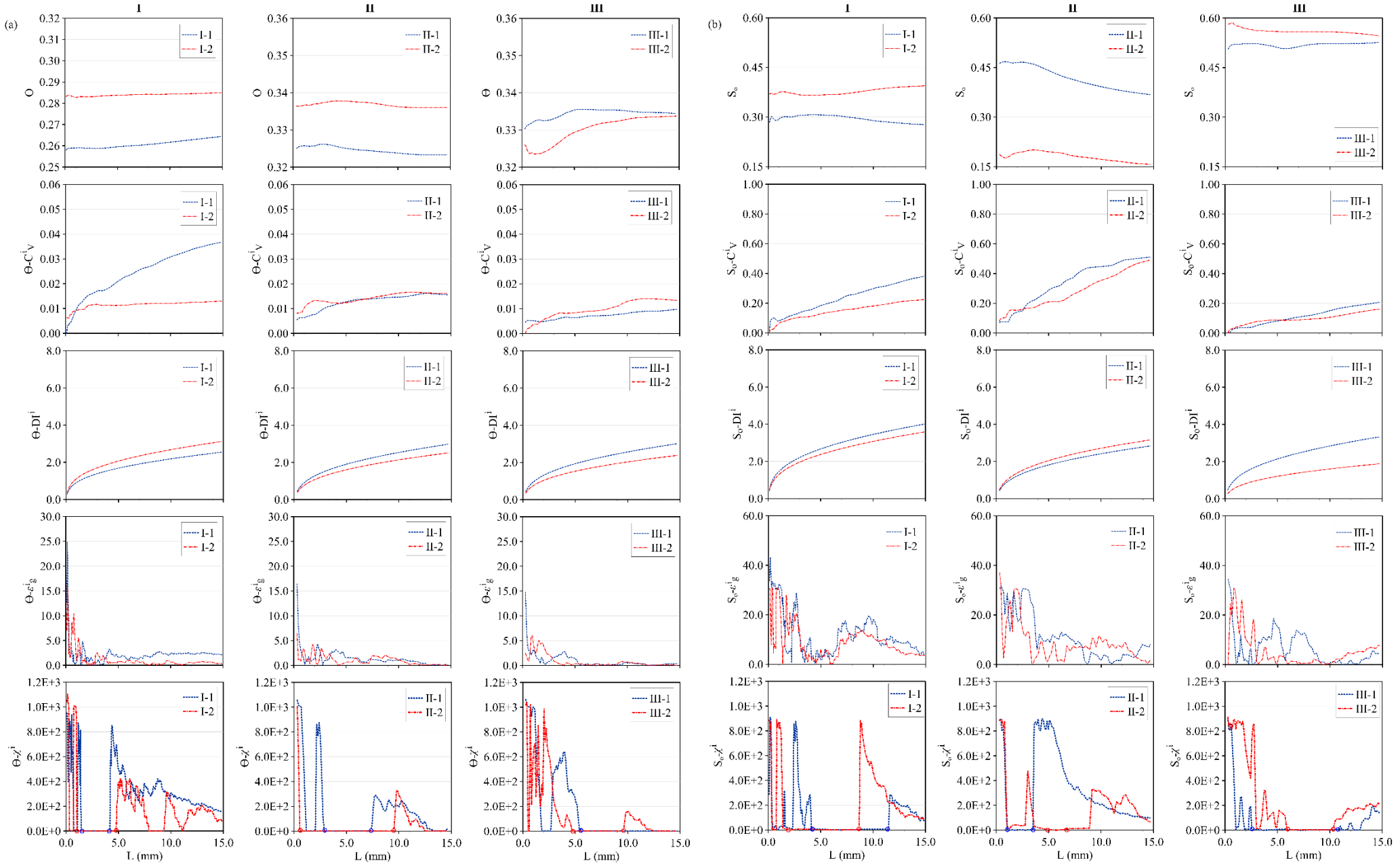
(a)
(b)
I
II
III
I-1
I-2
II-1
II-2
III-1
III-2
Θ
S_0
Θ-C^i_V
S_0-C^i_V
Θ-DI^i
S_0-DI^i
Θ-ε^i_g
S_0-ε^i_g
Θ-χ^i
S_0-χ^i
L (mm)

Fig. 5

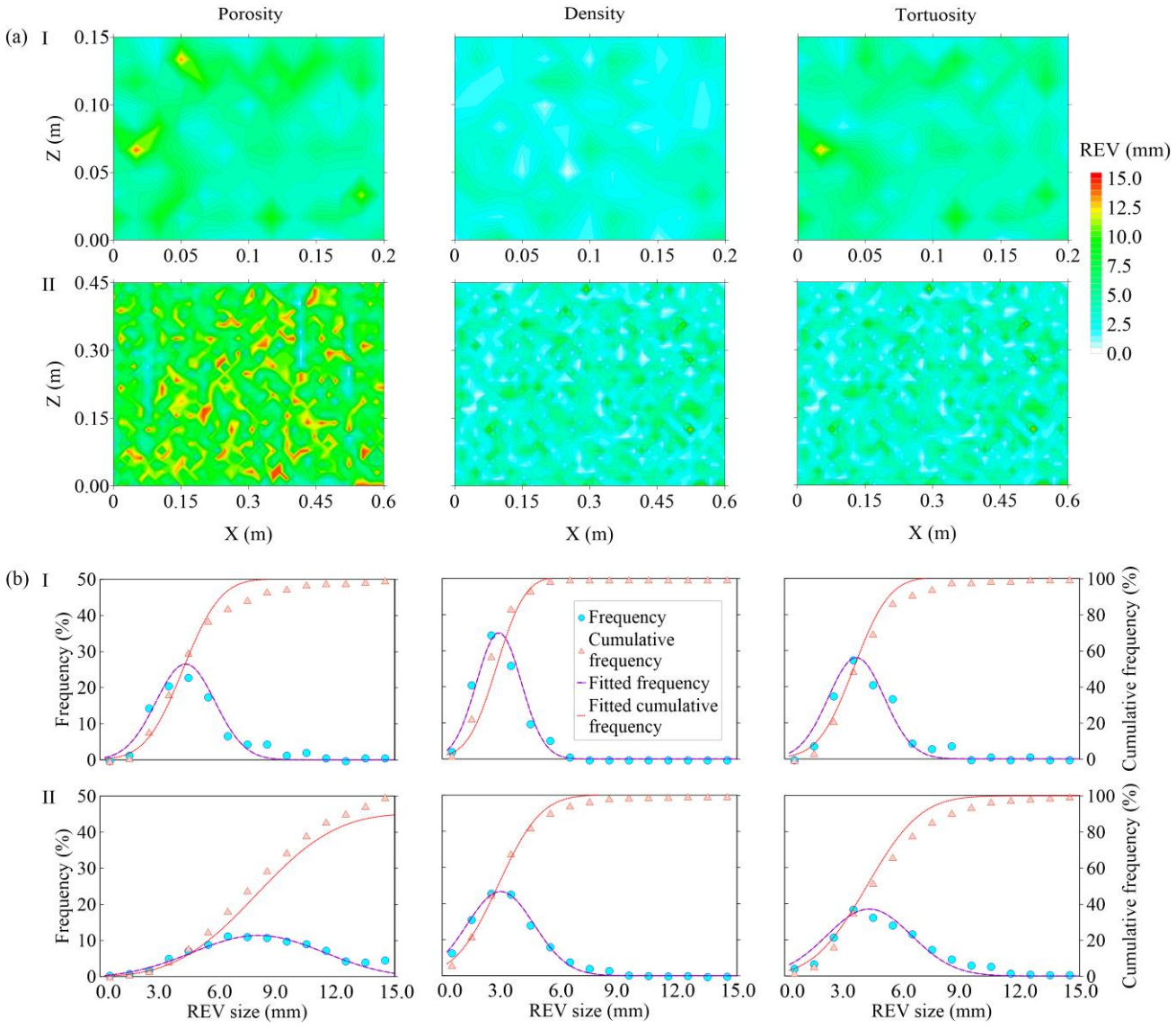
Porosity
Density
Tortuosity
(a) I
II
Z (m)
X (m)
REV (mm)
15.0
12.5
10.0
7.5
5.0
2.5
0.0
(b) I
II
Frequency (%)
Cumulative frequency (%)
REV size (mm)
Frequency
Cumulative frequency
Fitted frequency
Fitted cumulative frequency

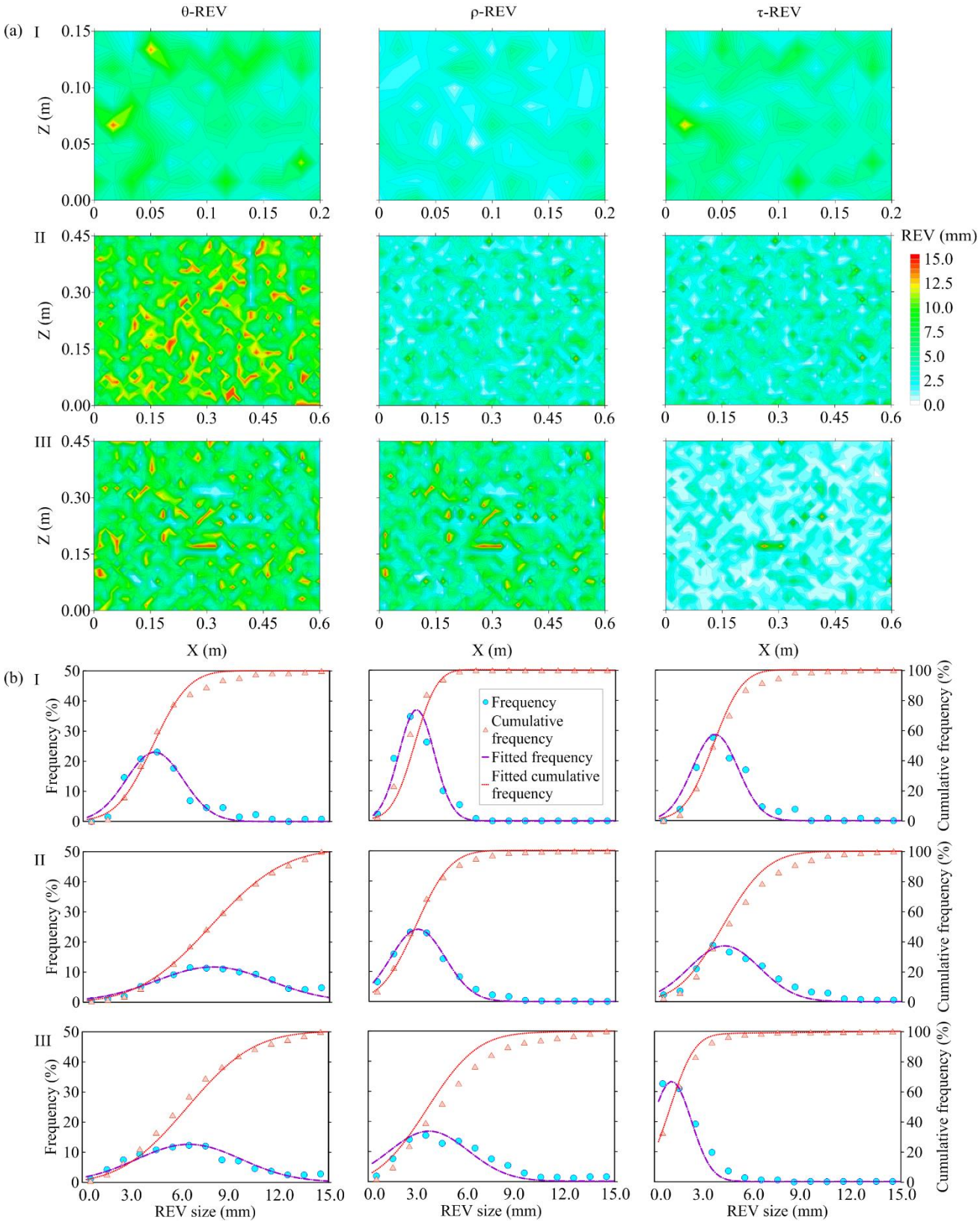
(a)
θ-REV
ρ-REV
τ-REV
I
II
III
Z (m)
REV (mm)
15.0
12.5
10.0
7.5
5.0
2.5
0.0
X (m)
(b)
Frequency (%)
Cumulative frequency (%)
Frequency
Cumulative frequency
Fitted frequency
Fitted cumulative frequency
REV size (mm)

Fig. 6

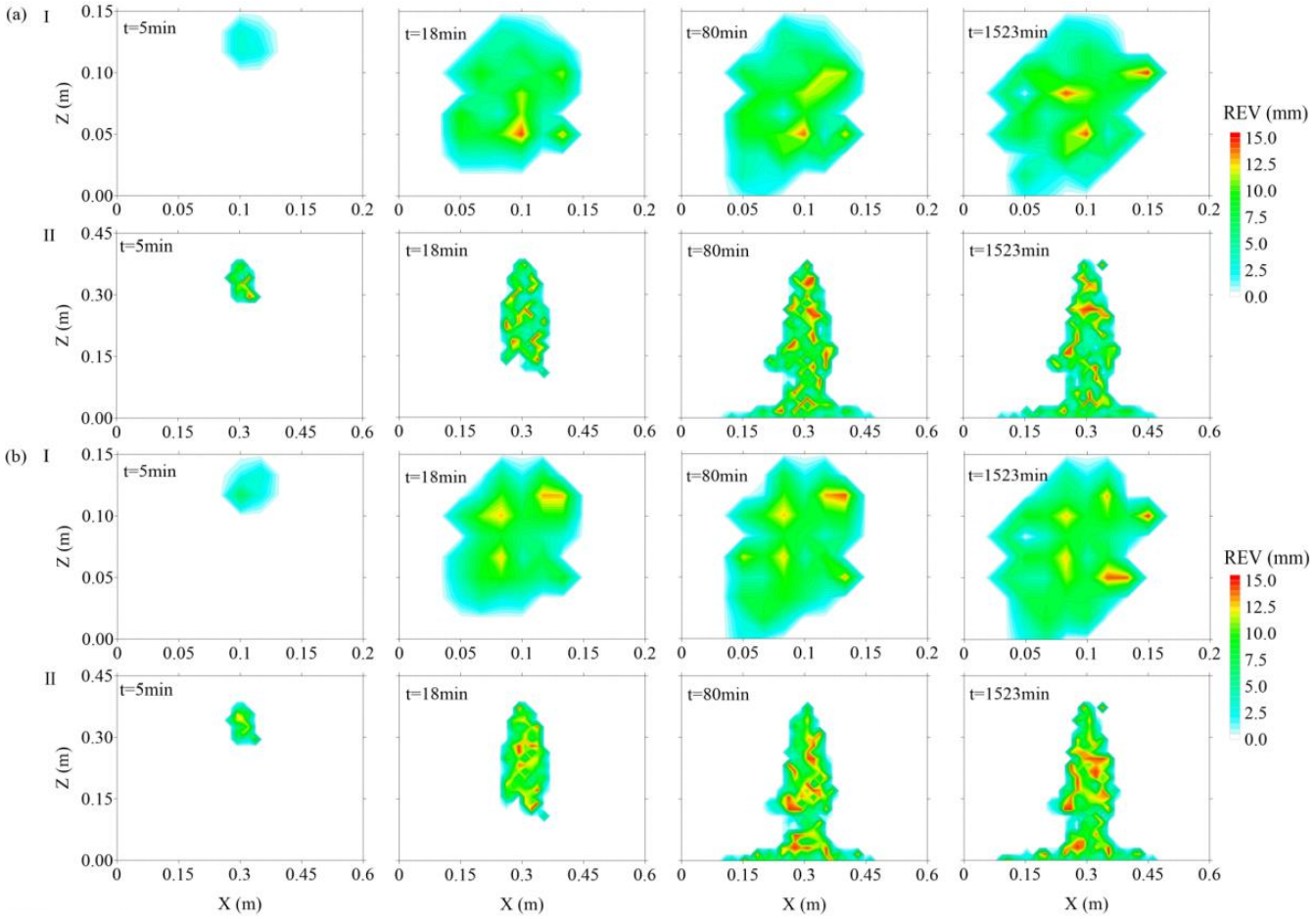
(a) I
t=5min
t=18min
t=80min
t=1523min
Z (m)
II
(b) I
X (m)
REV (mm)
15.0
12.5
10.0
7.5
5.0
2.5
0.0

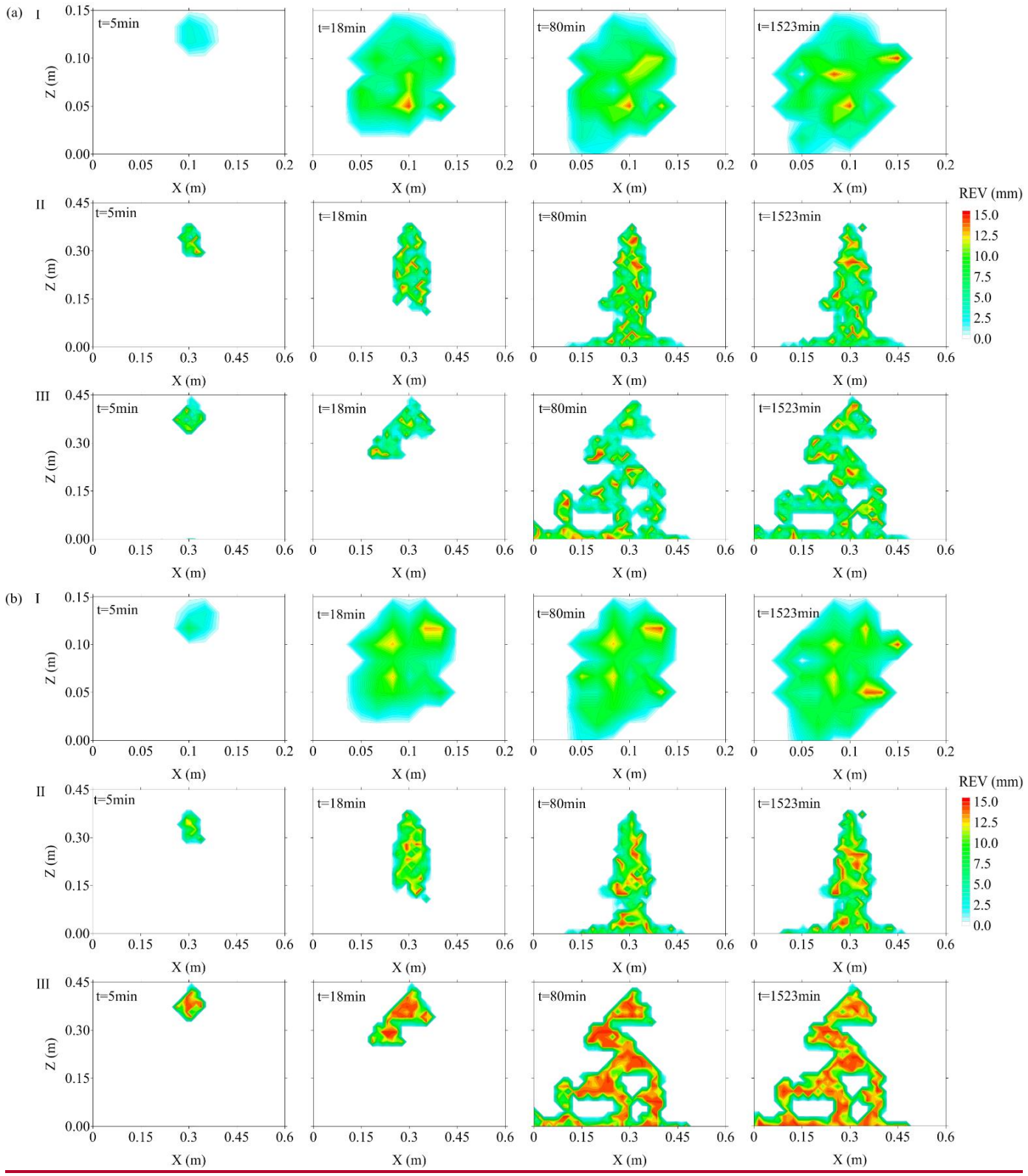
(a)
I
II
III
t=5min
t=18min
t=80min
t=1523min
Z (m)
X (m)
REV (mm)
15.0
12.5
10.0
7.5
5.0
2.5
0.0
(b)
I
II
III
t=5min
t=18min
t=80min
t=1523min
Z (m)
X (m)
REV (mm)
15.0
12.5
10.0
7.5
5.0
2.5
0.0

Fig. 7

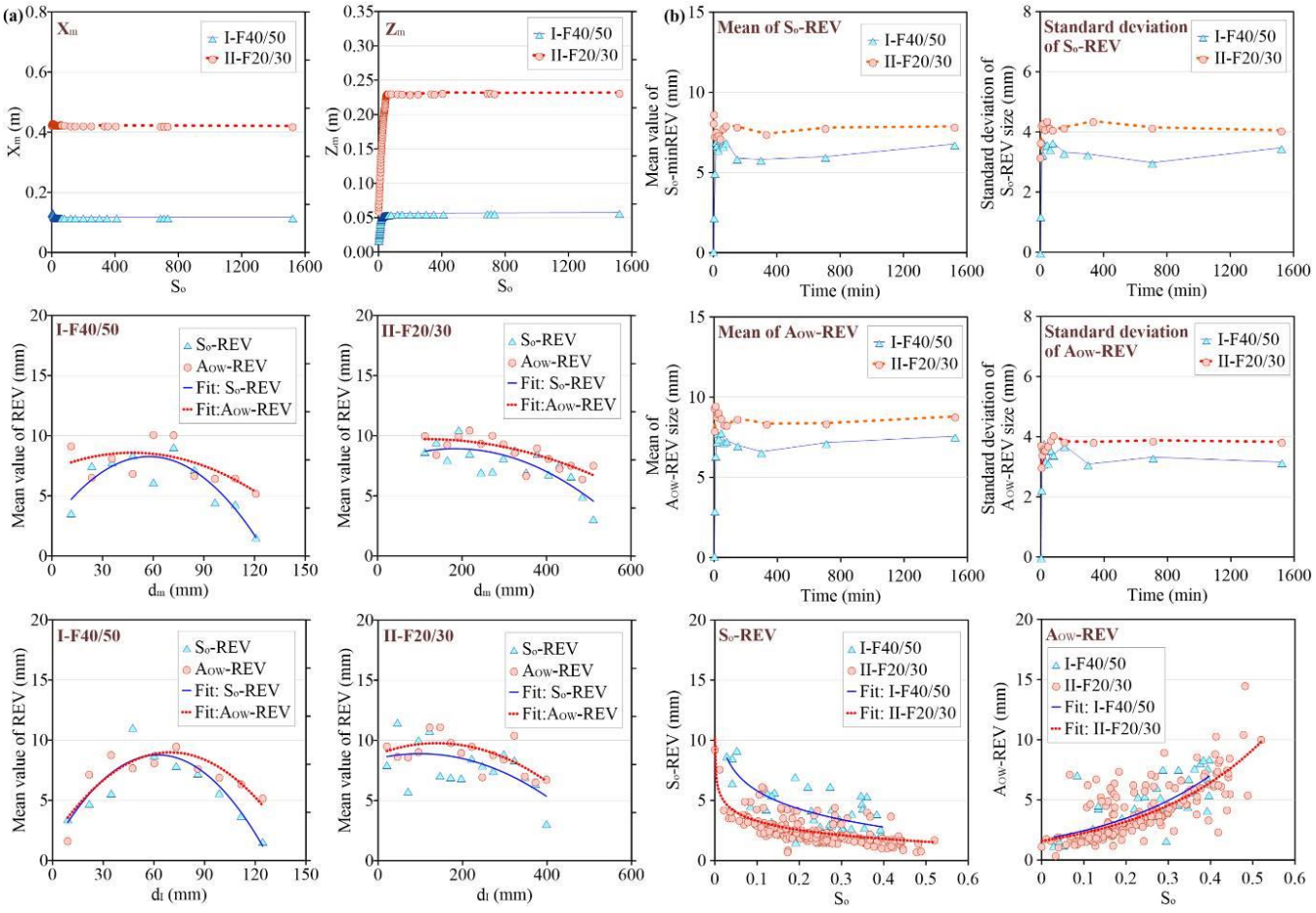
(a)
Xm
I-F40/50
II-F20/30
Xm (m)
So
Zm
Zm (m)
(b)
Mean of So-REV
Mean value of So-minREV (mm)
Time (min)
Standard deviation of So-REV
Standard deviation of So-REV size (mm)
I-F40/50
II-F20/30
So-REV
Aow-REV
Fit: So-REV
Fit:Aow-REV
Mean value of REV (mm)
dm (mm)
Mean of Aow-REV
Mean of Aow-REV size (mm)
Standard deviation of Aow-REV
Standard deviation of Aow-REV size (mm)
dt (mm)
Fit: I-F40/50
Fit: II-F20/30
Aow-REV (mm)

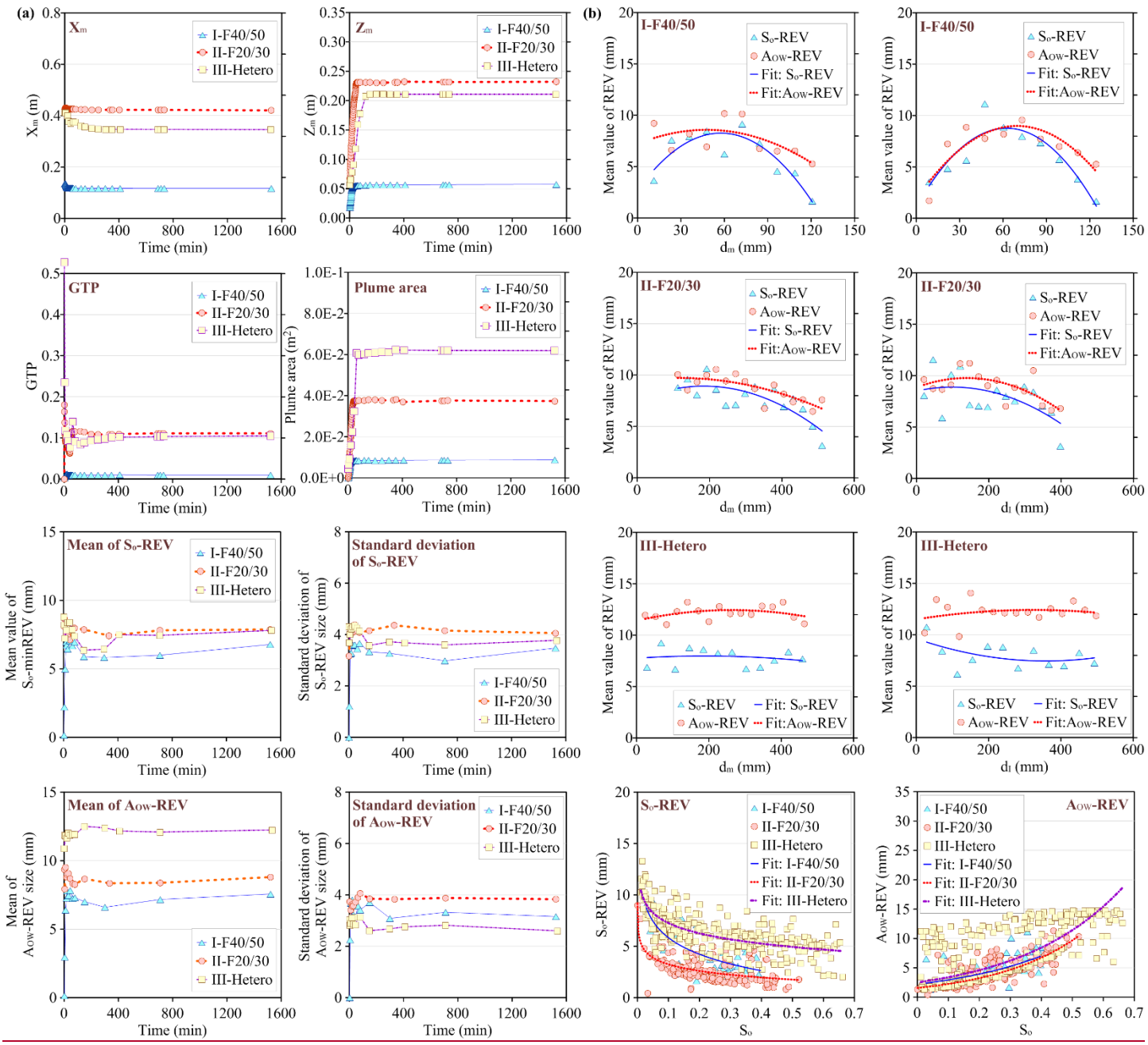
(a)
Xm
Zm
GTP
Plume area
Mean value of So-REV
Standard deviation of So-REV
Mean of Aow-REV
Standard deviation of Aow-REV
I-F40/50
II-F20/30
III-Hetero
Time (min)
(b)
So-REV
Aow-REV
Fit: So-REV
Fit:Aow-REV
Mean value of REV (mm)
dm (mm)
dl (mm)
Fit: I-F40/50
Fit: II-F20/30
Fit: III-Hetero
So

716